

Paleoliquefaction in Christchurch, New Zealand

Sarah H. Bastin[†], Mark C. Quigley, and Kari Bassett

Department of Geological Sciences, University of Canterbury, Christchurch 8014, New Zealand

ABSTRACT

Liquefaction during the 2010 moment magnitude (M_w) 7.1 Darfield earthquake and large aftershocks (known as the Canterbury earthquake sequence) caused severe damage to land and infrastructure in Christchurch, New Zealand. Liquefaction occurred at M_w -weighted peak ground accelerations ($PGA_{7.5}$) as low as 0.06g at highly susceptible sites. Trenching investigations conducted at two sites in eastern Christchurch enabled documentation of the geologic expressions of recurrent liquefaction and determination of whether evidence of pre-Canterbury earthquake sequence liquefaction is present. Excavation to water table depths (~1–2 m below surface) across sand blow vents and fissures revealed multiple generations of Canterbury earthquake sequence liquefaction “feeder” dikes that crosscut Holocene-to-recent fluvial and anthropogenic stratigraphy. Canterbury earthquake sequence dikes crosscut and intrude oxidized and weathered dikes and sills at both sites that are interpreted as evidence of pre-Canterbury earthquake sequence liquefaction. Crosscutting relationships combined with ¹⁴C dating constrain the timing of the pre-Canterbury earthquake sequence liquefaction to post-A.D. 1660 to pre-ca. A.D. 1905 at one site, and post-A.D. 1415 to pre-ca. A.D. 1910 at another site. The $PGA_{7.5}$ of five well-documented historical earthquakes that caused regional damage between 1869 and 1922 are approximated for the study sites using a New Zealand specific ground motion prediction equation. Only the June 1869 M_w ~4.8 Christchurch earthquake produces a median modeled $PGA_{7.5}$ that exceeds the $PGA_{7.5}$ 0.06g threshold for liquefaction. Prehistoric earthquakes sourced from regional faults, including the 1717 Alpine fault M_w ~7.9 ± 0.3 and ca. 500–600 yr B.P. M_w ≥ 7.1 Porters Pass fault earthquakes, provide additional potential paleoseismic sources for pre-Canterbury earthquake sequence liquefaction. The recognition of pre-Canterbury

earthquake sequence liquefaction in late Holocene sediments is consistent with hazard model-based predicted return times of PGAs exceeding the liquefaction triggering threshold in Christchurch. Residential development in eastern Christchurch from ca. 1860 to 2005 occurred in areas where geologic evidence for pre-Canterbury earthquake sequence liquefaction was present, highlighting the potential of paleoliquefaction studies to predict locations of future liquefaction and to contribute to seismic hazard assessments and land-use planning.

INTRODUCTION

Cyclic shearing of loosely compacted and fluid-saturated sediments during earthquake-induced ground motion results in excess pore-water pressures and reduced shear strength in the affected media. Sediment transitions to a liquefied state as excess pore-water pressures exceed the static confining pressure, causing large strains and flowage of the sediment, and breakdown of the grain arrangement (Seed and Idriss, 1982; Idriss and Boulanger, 2008). Liquefied sediment may be ejected to the ground surface via feeder dikes, that commonly utilize fractures in the sedimentary cover overlying the liquefied stratum. Surface ejecta commonly manifests as sand blows, blistering of the surface by near-surface sediment injection, and vertical (subsidence) or lateral (lateral spreading) ground deformation (Seed and Idriss, 1982; Sims and Garvin, 1995; Tuttle and Barstow, 1996; Obermeier, 1996; Galli, 2000; Idriss and Boulanger, 2008; Cubrinovski and Green, 2010; Tuttle and Hartleb, 2012; Quigley et al., 2013). Surface liquefaction features may be rapidly (i.e., within hours to months) reworked into forms that are difficult to distinguish from eolian, fluvial, or estuarine deposits (Sims and Garvin, 1995; Reid et al., 2012; Quigley et al., 2013), complicating the geologic identification of prehistoric features. However, subsurface liquefaction features such as dikes, laterally injected sills, and other injection features are commonly present in the geologic record where host sediments are

preserved, enabling the detection of historic or prehistoric (i.e., paleoliquefaction) events (Obermeier, 1996; Obermeier et al., 2005; Tuttle et al., 2006). Paleoliquefaction features ranging in age from 10² yr (Sims and Garvin, 1995) to several 10⁸ yr (Loope et al., 2013) have been identified from geologic investigations.

Paleoliquefaction provides evidence for paleoearthquakes with site-specific strong ground motions and shaking durations that exceeded threshold values for liquefaction (Green et al., 2005). Analysis of paleoliquefaction features preserved in the geologic record may enable recurrence intervals, ground motions, and magnitudes of the paleoearthquakes to be estimated (Obermeier et al., 1991; Obermeier, 1996; Tuttle et al., 2002; Green et al., 2005; Tuttle and Atkinson, 2010). Paleoliquefaction investigations rely on the accurate identification of features, interpretation of their relative ages, and constraints on the shaking intensities under which liquefaction was triggered (Obermeier et al., 1991; Sims and Garvin, 1995; Obermeier, 1996; Tuttle, 2001; Tuttle et al., 2002). The minimum peak ground acceleration (PGA) required to trigger liquefaction is typically determined for a site using site-specific geotechnical tests (i.e., cone penetration tests [CPT], standard penetrations tests [SPT], and Swedish weight sounding [SWS]; Seed and Idriss, 1982; Idriss and Boulanger, 2008). Seismic triggering thresholds for initiating liquefaction are typically characterized using moment magnitude-weighted $PGA_{7.5}$ (Green et al., 2005; Quigley et al., 2013). A $PGA_{7.5}$ value represents the equivalent PGA for a M_w 7.5 event. This is calculated from a magnitude scaling factor (MSF) that accounts for the shaking duration and frequency content of the ground motion ($PGA_{7.5} = PGA \times 1/MSF$; Idriss and Boulanger, 2008). Recent compilations of earthquake and liquefaction data suggest a liquefaction-inducing threshold of $PGA_{7.5} = 0.09g$ (Santucci de Magistris et al., 2013), although minor liquefaction has been reported in highly susceptible sediments under $PGA_{7.5}$ as low as ~0.06g (Quigley et al., 2013). Sedimentary (e.g., grain size, clay content) and hydrologic characteristics

[†]sarah.bastin@pg.canterbury.ac.nz

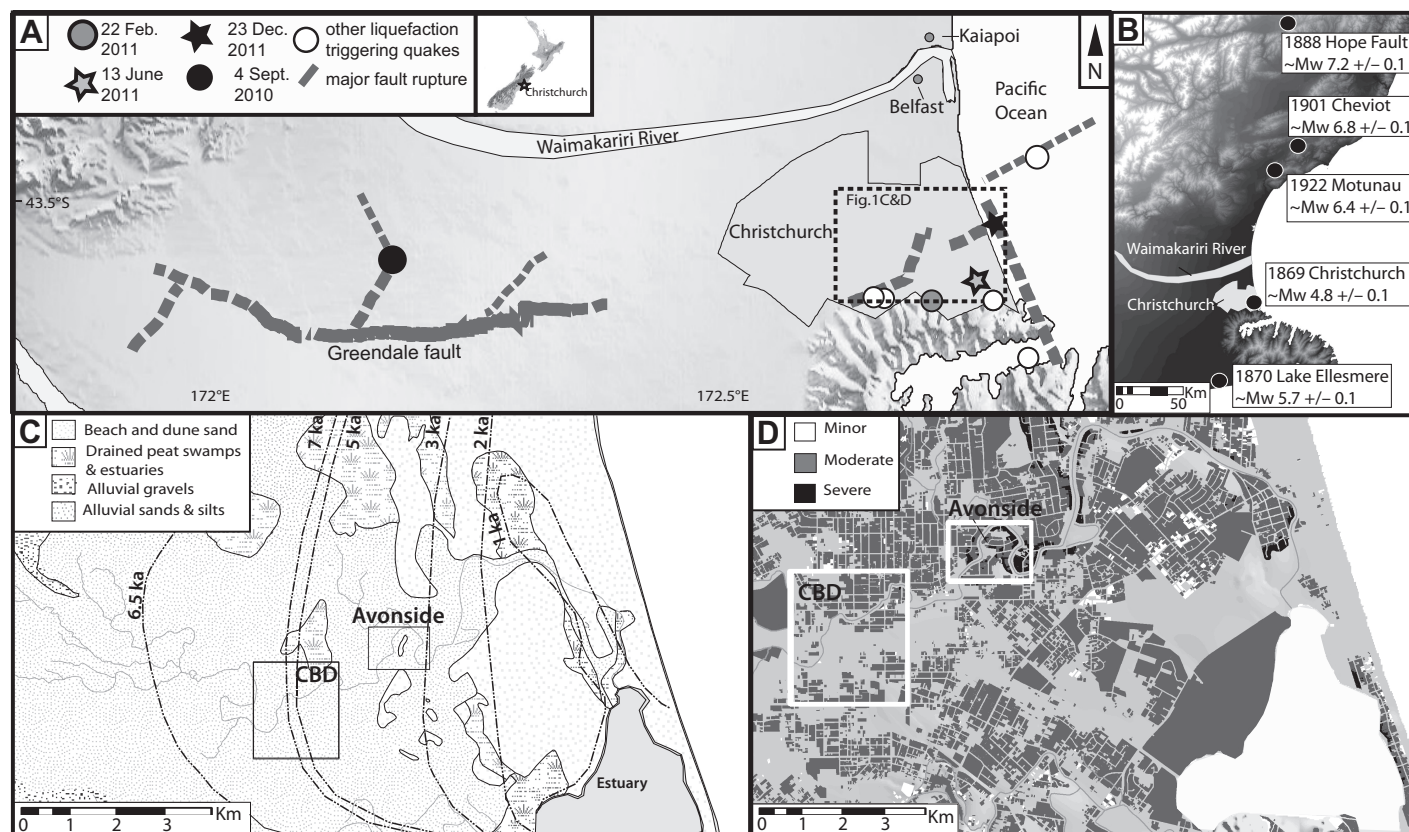


Figure 1. (A) Epicentral locations of the 2010–2011 Canterbury earthquake sequence that generated liquefaction within Avonside. The rupture of the Greendale fault (bold line) and projected locations of the subsurface faults (dashed lines) that ruptured in the February, June, and December 2011 aftershocks are indicated (modified from Quigley et al., 2013). (B) The approximate epicenter location of the five historic earthquakes causing damage within the wider Christchurch area from 1869 to 1922. Pre-Canterbury earthquake sequence liquefaction was reported in Kaiapoi and Belfast (indicated) following the 1901 Cheviot earthquake. (C) Simplified geological map of the Christchurch area (modified from Brown and Weeber, 1992), with the approximate locations of the 7–1 ka shorelines indicated with respect to Avonside and the Central Business District (CBD). (D) The spatial extent and severity of liquefaction as mapped following the 22 February 2011 earthquake.

(e.g., water table depth) of the source sediment influence liquefaction susceptibility.

The 2010–2011 Canterbury earthquake sequence caused at least 10 distinct episodes of observed liquefaction in parts of eastern Christchurch, New Zealand (Quigley et al., 2013). The most severe liquefaction-induced damage was reported following the September 2010 M_w 7.1 Darfield main shock, and the February 2011 M_w 6.2 (i.e., 2011 Christchurch earthquake), June 2011 M_w 6.0, and December 2011 M_w 5.9 aftershock earthquakes (Fig. 1; Cubrinovski and Green, 2010; Cubrinovski et al., 2011; Quigley et al., 2013). As a result of extensive land and infrastructure damage, more than 6000 residential properties in eastern Christchurch were purchased by the central government (<http://cera.govt.nz/residential-red-zone>). Recent estimates of post-insurance pay-out losses exceed \$NZ 1 billion (\$U.S. 800 million; <http://www.stuff.co.nz/national/christchurch-earthquake/8655455/Govt-faces>

-1-billion-red-zone-shortfall). Understanding the timing, location, magnitude, and frequency of liquefaction-inducing earthquakes in Christchurch (e.g., Almond et al., 2013; Bastin et al., 2013) thus has the potential to inform land-use planning decisions and make contributions to seismic hazard modeling (e.g., Stirling et al., 2012).

Pre-Canterbury earthquake sequence liquefaction was reported in Kaiapoi and Belfast (Fig. 1B) following the 1901 M_w 6.8 Cheviot earthquake (Berrill et al., 1994); however, no pre-Canterbury earthquake sequence liquefaction had been recorded in Christchurch. In this study, we first describe the subsurface morphology of Canterbury earthquake sequence liquefaction features at two study sites, with the goals of (1) documenting how this earthquake sequence is manifested in the geologic record, and (2) characterizing the source layer of contemporary liquefaction. We then present new stratigraphic and chronologic evidence

for previously undocumented pre-Canterbury earthquake sequence liquefaction in eastern Christchurch.

GEOLOGIC SETTING

Christchurch Area

The city of Christchurch (population ~360,000) is primarily situated upon a low-relief and low-elevation alluvial landscape (0–20 m above sea level) on the east coast of New Zealand's South Island (Fig. 1). The city and eastern suburbs are predominantly underlain by drained peat swamps, fluvial sands and silts, and estuarine, dune, and foreshore sands (Fig. 1C; Brown and Weeber, 1992). Channelized gravels in the uppermost several meters are typically attributed to deposition by the braided Waimakariri River that intermittently avulsed through the city prior to European settlement (Fig. 1; Cowie, 1957; Brown and Weeber, 1992). To the west of

the central city, fluvial sands and gravels predominate (Fig. 1C).

The sediments in eastern Christchurch were deposited by shoreline progradation and marine regression following the mid-Holocene highstand with shorelines recorded ~3 km west of the present central city at ~6500 yr B.P. (Fig. 1C; Brown and Weeber, 1992). The fluvial sands and silts reflect deposition by the meandering Avon and Heathcote Rivers within the city (Fig. 1C). The youthful, unconsolidated nature of the fine sands to silt underlying eastern Christchurch combined with high water tables (1–2 m depth) and localized artesian water pressures pose a long-recognized high liquefaction hazard (Elder et al., 1991). This was confirmed during the Canterbury earthquake sequence (Cubrinovski and Green, 2010). Liquefaction may also have been exacerbated in parts of the eastern suburbs by leakage of underlying artesian aquifers through breached aquitards (Cox et al., 2012).

Avonside Study Area

The study area of Avonside, eastern Christchurch, experienced severe liquefaction-induced damage during the Canterbury earthquake sequence (Fig. 1D). Avonside is encompassed within an inner meander bend of the Avon River, which undergoes tidally influenced flow inversions (Fig. 1C). The suburb is underlain by fine sand and silt of point bar and overbank deposits of the Avon River, along with coastal swamp and sand dune deposits (Fig. 1C; Silby, 1856; Brown and Weeber, 1992). Localized channelized gravels that are present at ~2 m depth may be related to historic floods of the Waimakariri River through this area prior to European settlement (Brown and Weeber, 1992). The position of the ~5000 yr. B.P. coastline was ~3 km to the west, and the ~3000 yr. B.P. coastline was ~0.5–1 km east of the study sites (Fig. 1C; Brown and Weeber, 1992). The modern coastline is located ~5 km to the east (Fig. 1C). The water table is located between 1 and 2 m depth; however, it can rise to ≤0.5 m depth during wet periods (Brown and Weeber, 1992).

Two sites were chosen for trenching to investigate the morphology and stratigraphic relationships of the Canterbury earthquake sequence and pre-Canterbury earthquake sequence liquefaction features in the subsurface (Fig. 2A): Sullivan Park (site 1; Fig. 2B), and the former site of a residential property at 11 Bracken Street (site 2; Fig. 2D). Site 1 was selected based on the intensity of lateral spreading cracks and lack of near-surface anthropogenic influence on the spatial distribution of liquefaction (Fig. 2C). Site 2 was selected because it was continuously



Figure 2. (A) Digital elevation model (DEM) of the Avonside area with the location of the two study sites indicated. (B) Uninterrupted aerial photograph of site 1 following the February 2011 earthquake with trench and CPTu (cone penetration test with pore-pressure [piezocene] measurement) locations indicated. (C) The mapped distribution of liquefaction features, and locations of the trenches and CPTu at site 1. (D) Uninterrupted aerial photograph of site 2 following the February 2011 earthquake with the trench location indicated. (E) The mapped distribution of liquefaction ejecta following the February 2011 earthquake (modified from Quigley et al., 2013), with the locations of the trench and residential dwelling indicated.

monitored by Quigley et al. (2013) during the Canterbury earthquake sequence (Fig. 2E). Calibration of the observations for the occurrence and nonoccurrence of liquefaction with nearby accelerometer measurements of PGA enabled a $PGA_{7.5}$ liquefaction triggering threshold to be established for the susceptible sediments at site 2 of $PGA_{7.5} \sim 0.06g$ (minor liquefaction) to $PGA_{7.5} 0.12g$ (major to severe liquefaction; for a full description of $PGA_{7.5}$ derivation methodology for this study site, see Quigley et al., 2013).

METHODS

Trenching

The subsurface morphology of the Canterbury earthquake sequence and prior liquefaction features was documented using well-established criteria for identifying earthquake-induced liquefaction features, including analysis of aerial photography, trenching, and dating of subsurface deposits (e.g., Sims, 1975; Obermeier et al., 1991; Obermeier, 1996; Tuttle, 2001). Documentation of the subsurface features that fed known Canterbury earthquake sequence surface vents, and comparison with published photographs of subsurface liquefaction features aided the identification and interpretation of other liquefaction features that pinched out beneath the surface (see also Obermeier et al., 2005; Tuttle, 2001; Counts and Obermeier, 2012). High-resolution aerial photographs (flown on 24 February 2011 by NZ Aerial Mapping for the Christchurch Response Centre) were examined to identify the distribution of features at each site (Fig. 2). Trenches were excavated perpendicular to aligned sand blow vents and lateral spreading fissures at both sites (Fig. 2). Trench walls were cleaned using handheld scrapers and then photographed and logged at centimeter scale to document small-scale changes in the morphology of the liquefaction features and the surrounding stratigraphy. The trench floor was also logged at several locations of interest at site 1 (Fig. 3A). The documentation of Canterbury earthquake sequence liquefaction features and their relationship with the surrounding sediment enabled prior liquefaction features to be identified within the stratigraphy. The liquefaction features and the surrounding stratigraphy were described in terms of their grain size, sorting, color, and degree of sediment mottling. Full sediment descriptions of each unit are presented in Appendix 1.¹ Two hand-augered holes at

site 1 were excavated to 2.5 m depth, where the sediment became cohesionless and failed to be retained within the auger head.

Radiocarbon Dating

The ages of the pre-Canterbury earthquake sequence liquefaction features and trench stratigraphy were constrained from radiocarbon dating of detrital wood fragments obtained from key stratigraphic horizons. Samples were dried at 40 °C for 1 wk and then sorted to separate the organic material from the host sediment. Between 10 and 20 mg samples of organic material were submitted to the Rafter Radiocarbon Laboratory in Wellington, New Zealand, for accelerator mass spectrometry (AMS) radiocarbon analysis. Samples were prepared for analysis by subsampling, picking, and grinding of the wood fragments, and repeated acid and alkali treatment, after which they were combusted and converted to graphite by reduction with hydrogen over iron catalyst. Ages were calibrated using the Southern Hemisphere calibration curve (SHCAL04; McCormac et al., 2004). The radiocarbon ages referred to in the text are reported as 2σ calendar calibrated age ranges. The uncalibrated conventional radiocarbon ages and detailed age range distributions of the calendar calibrated ages are presented in Table 1.

Optically Stimulated Luminescence Dating

Two sediment samples were collected from site 1 for optically stimulated luminescence (OSL) dating to further constrain the likely depositional ages of the trench stratigraphy. Sampling was conducted by pushing 5-cm-diameter stainless-steel tubes into cleaned sections of the trench wall. Samples were dated by infrared stimulated luminescence (IRSL) of the polymineral fine grain fraction (4–11 mm) using a Riso TL-DA-15 with an infrared diode array at the OSL facility at the University of Victoria, Wellington, New Zealand. The equivalent dose was determined in the blue spectral band (filters BG39+Kopp 5–58) by the single-aliquot additive dose method with late light subtraction (SAR method; Aitken, 1998). The multiple aliquot additive dose method (MAAD) was applied to determine the dose rate. Radionuclide contents of ^{238}U , ^{232}Th , and ^{40}K , a values, and water content were measured from a sample aliquot. Samples were stored for 3 wk after irradiation, and a 5 min preheat was then applied to isolate the stable signal component. After 6 mo of storage, samples were subjected to a fading test. All measurements were conducted at room temperature (Aitken, 1998). Optical ages are presented in Table 2.

Geotechnical Testing

A CPTu (cone penetration test with pore-pressure [piezocone] measurement) was conducted ~20 m north of trench 1 at site 1 to a depth of 20 m (Fig. 2B). The CPTu measures the resistance of the subsurface sediments to an instrumented cone being pushed at a constant rate (Idriss and Boulanger, 2008). The relative resistance of the subsurface sediments acts as a proxy for the subsurface properties and for delineating stratigraphy. The CPTu is commonly applied to determine the liquefaction susceptibility of a given area due to its rapid testing times, continuous recording, high accuracy, and the repeatability of the test (Idriss and Boulanger, 2008).

The liquefaction potential of the subsurface strata was evaluated from the CPTu using the Idriss and Boulanger (2008) method. This method establishes the liquefaction potential by comparing the cyclic stress ratio (CSR), which evaluates loading induced at different depths by an earthquake, with the cyclic resistance ratio (CRR), which represents the ability of the soil to resist liquefaction. The likelihood that a soil will liquefy is expressed as a factor of safety against liquefaction (FS), where $FS < 1$ is considered potentially liquefiable. The results of the CPTu sounding were correlated with the stratigraphy to 2.5 m depth, as determined from the trench and hand auger. This enabled the possible depth of the liquefied source sediment to be constrained.

SITE 1: SULLIVAN PARK

Sullivan Park is located centrally within Avonside and within 50 m of the Avon River (Fig. 2). The park has almost flat topography with elevations of 1.5–2 m above sea level across the site (Fig. 2). Analysis of the post-February 2011 aerial photographs indicates that lateral spreading-induced fissuring and associated sand blows formed across the site during the Canterbury earthquake sequence (Fig. 2C).

Three trenches (T1–T3) were excavated perpendicular to the axis of two lateral spreading fissures to lengths of ~18 m (T1), ~6 m (T2), and ~8 m (T3) and a depth of ~1.5 m (Fig. 2B). The trench excavation depth was limited to ~1.6 m by the depth of the water table. Two hand-augered holes were excavated in T1 and T2 (A1 and A2, respectively) to a depth of 2.5 m. The trench and auger logs are presented in Figures 3, 4, 5, and 7, and selected field photographs are presented in Figures 6 and 8. The CPTu data is presented in Figure 9.

¹GSA Data Repository item 2015131, Appendix 1: Detailed sedimentary descriptions, is available at <http://www.geosociety.org/pubs/ft2015.htm> or by request to editing@geosociety.org.

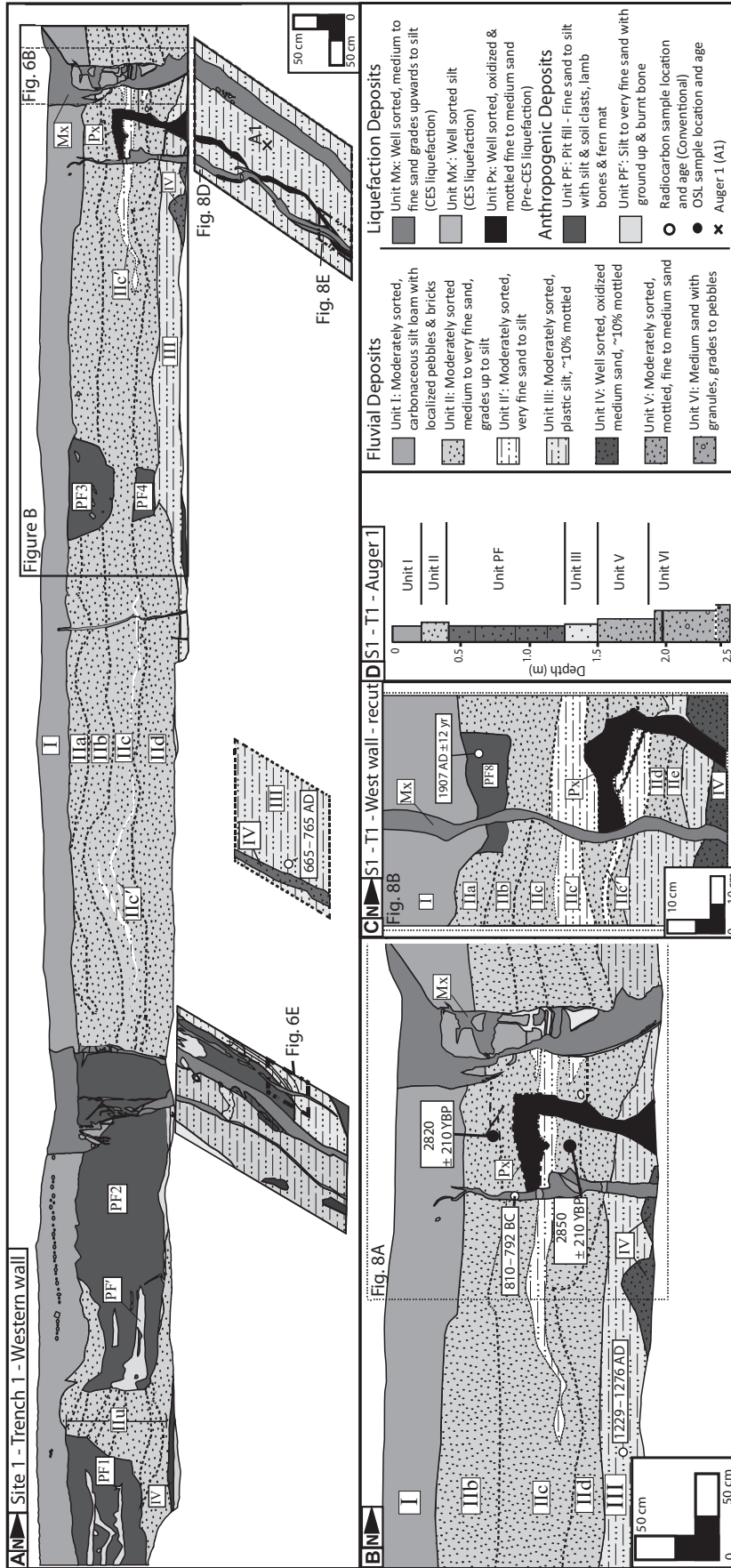


Figure 3. (A) Detailed trench log of the west wall and floor of T1 (site 1). The Canterbury earthquake sequence (CES) liquefaction dikes (Mx) crosscut the fluvial (I–III) and anthropogenic (PF1–PF4) stratigraphy. The pre–Canterbury earthquake sequence dike (Px) is cross-cut by a Canterbury earthquake sequence dike (Mx) and dissipates within bed of fluvial sand (IIc). The location of auger 1 (A1) is also indicated. (B) Close-up of the crosscutting relationship between the Canterbury earthquake sequence (MX) and oxidized dike (PX). The locations and results of the ¹⁴C and optically stimulated luminescence (OSL) samples are indicated. (C) Detailed log of the re-cut of the trench wall. The Canterbury earthquake sequence dike (Mx) crosscuts the fluvial (I–III) and anthropogenic (P8) stratigraphy and the pre–Canterbury earthquake sequence dike (Px), which dissipates into the fluvial sand (unit IIc). (D) Auger 1 (1.5–2.5 m) indicates the trench is underlain by moderately sorted, fine to medium sand (unit V) that contains granules to pebbles (unit VI) from 1.9 to 2.5 m depth.

TABLE 1. RADIOCARBON DATA AND AGE ESTIMATES

Sample no.	Depth (m)	Locality	Description	$\delta^{13}\text{C}$ (‰)	Radiocarbon age (yr B.P.)		Calendar calibrated age	
					1σ	2σ	1σ	2σ
S1	0.8	Trench 3 Site 1	Wood fragment from fluvial sand (unit IIc)	-26.4 ± 0.2	4126 ± 25	2858–2807 B.C. (17.1% of area)	2834–2814 B.C. (10.6% of area)	
						2752–2719 B.C. (5.8% of area)	2670–2571 B.C. (55.7% of area)	
						2701–2562 B.C. (64.1% of area)	2509–2504 B.C. (1.7% of area)	
SS2	0.9	Trench 3 Site 1	Wood fragment from fluvial sand (unit IIc)	-27.1 ± 0.2	220 ± 19	1660–1684 A.D. (17.3% of area)	1669–1675 A.D. (6.9% of area)	
						1730–1803 A.D. (77.4% of area)	1739–1787 A.D. (56.2% of area)	
S3	1.40	Trench 1 Site 1	Wood fragment from basal silt (unit III)	-32.3 ± 2.0	813 ± 38	1229–1276 A.D.	1203–1295 A.D.	
						665–694 A.D. (46.6% of area)	660–721 A.D. (68.1% of area)	
S4	1.55	Trench 1 Site 1	Wood fragment from basal silt (unit III)	-24.9 ± 0.2	1364 ± 15	705–706 A.D. (0.9% of area)	742–770 A.D. (26.7% of area)	
						749–765 A.D. (20.2% of area)		
S5	0.20	Trench 1 Site 1	Fern sample from pit	-22.3 ± 0.2	111 ± 14	1709–1721 A.D. (4.7% of area)	1817–1830 A.D. (22.2% of area)	
						1811–1838 A.D. (29.9% of area)	1894–1921 A.D. (46.2% of area)	
S6	1.8	Pit 9 Site 1	Charcoal sample from pit 9	-26.4 ± 0.2	815 ± 20	1223–1279 A.D.	1230–1252 A.D. (41.9% of area)	
						810–792 B.C.	1261–1275 A.D. (27.7% of area)	
S7	1.15	Trench 1 Site 1	Wood fragment from Canterbury earthquake sequence dike	-26.5 ± 0.2	2683 ± 16	810–792 B.C.	828–779 B.C.	
						1415–1435 A.D.	1408–1442 A.D.	
S8	0.50	Trench 4 Site 2	Wood fragment from silt loam	-26.3 ± 0.1	545 ± 18			
S9	1.10	Trench 4 Site 2	Wood fragment from silt loam	-23.7 ± 0.1	606 ± 18	1330–1331 A.D. (1.3% of area)	1324–1346 A.D. (21.6% of area)	
						1392–1412 A.D. (65.8% of area)	1389–1418 A.D. (73.1% of area)	

TABLE 2. OPTICALLY STIMULATED LUMINESCENCE DATA AND AGE ESTIMATES

Laboratory no.	Sample no.	Locality	Depth (m)	Water (%)	K (%)	Radionuclide concentrations				Cosmic dose rate (Gy/ka)	D_e (Gy $^{-1}$)	Dose rate (Gy/ka)	Optical age (yr B.P.)	
						Th (ppm) from ^{208}Tl , ^{212}Pb , ^{228}Ac	U (ppm) from ^{232}Th	U (ppm) from ^{226}Ra , ^{214}Pb , ^{214}Bi	U (ppm) from ^{210}Pb					a-value
WLL1075	O1	Trench 1 Site 1	1.05	21.2 \pm 0.05	2.22 \pm 0.05	10.88 \pm 0.18	3.00 \pm 0.37	3.02 \pm 0.22	3.66 \pm 0.32	0.13 \pm 0.01	0.1797 \pm 0.0090	13.21 \pm 0.57	4.64 \pm 0.28	2850 \pm 210
						2.24 \pm 0.05	3.42 \pm 0.26	2.99 \pm 0.15	3.32 \pm 0.23	0.09 \pm 0.01	0.1845 \pm 0.009	11.95 \pm 0.62	4.24 \pm 0.23	2820 \pm 210
WLL1076	O2	Trench 1 Site 1	0.86	21.2 \pm 0.05	2.24 \pm 0.05	10.54 \pm 0.14	3.42 \pm 0.26	2.99 \pm 0.15	3.32 \pm 0.23	0.09 \pm 0.01	0.1845 \pm 0.009	11.95 \pm 0.62	4.24 \pm 0.23	2820 \pm 210

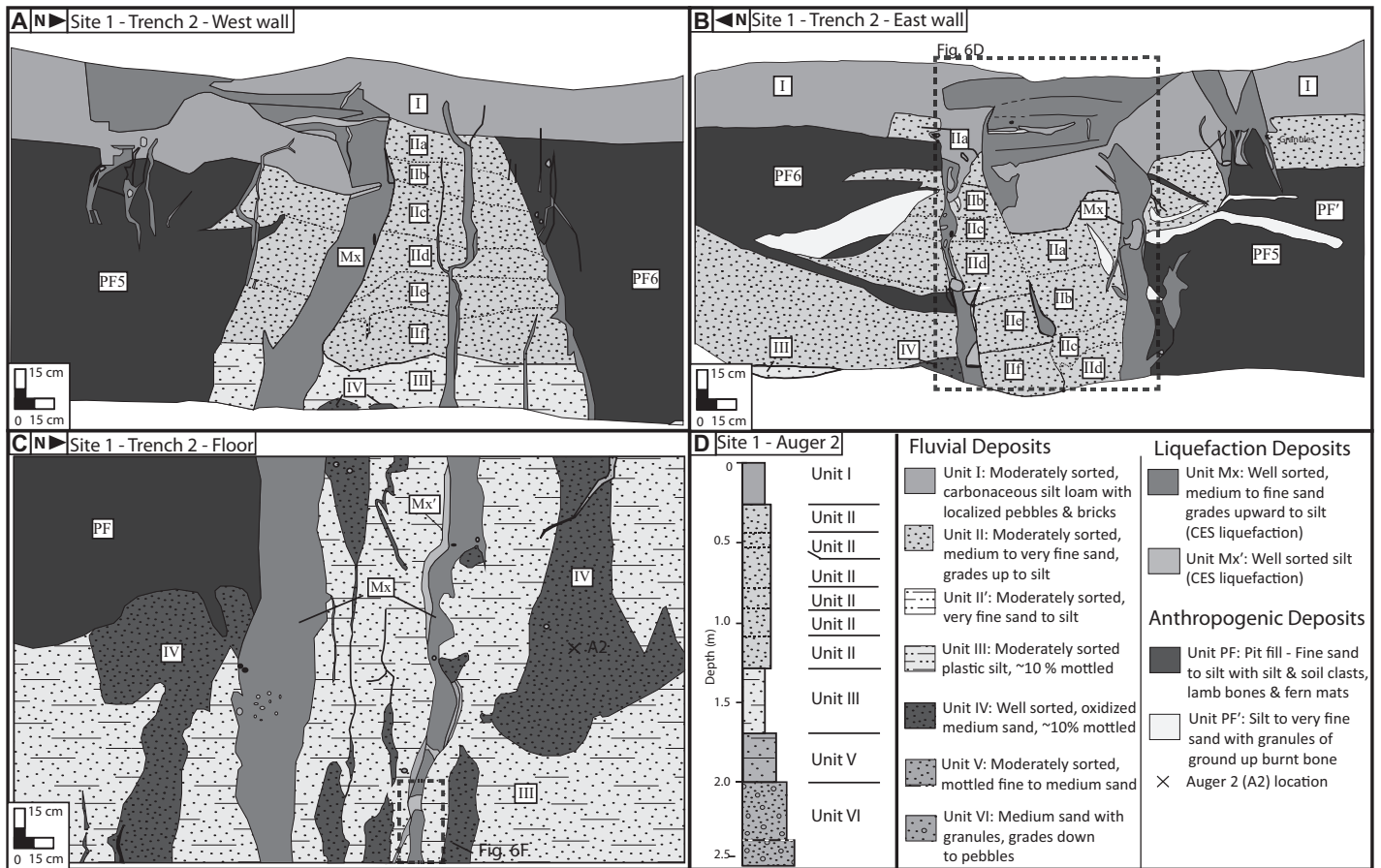


Figure 4. Detailed trench log of the west (A) and east (B) walls, and floor (C) of T2 (site 1). The location of auger 2 (A2) is also indicated. The Canterbury earthquake sequence (CES) liquefaction dikes (Mx) crosscut the fluvial stratigraphy (I–III) and anthropogenic cesspits (PF5–PF6) from the trench floor to surface. Small Canterbury earthquake sequence dikes (~10 cm long; Mx) are observed to originate within PF5 (A). (D) Auger 2 (1.5–2.5 m) indicates that the stratigraphy is underlain by moderately sorted fine to medium sand (unit V), that contains granules to pebbles (unit VI) from 2.3 to 2.5 m depth.

Trench Fluvial Stratigraphy

The three trenches (T1–T3; Figs. 3, 4, and 5) exposed stratigraphy composed of a plastic silt (unit III) with interbedded lenses of fine to medium sand (unit IV), overlain by normally graded beds of fine sand to silt (unit IIa–e). The stratigraphy is capped by ~20–50 cm of topsoil (unit I; Appendix 1 [see footnote 1]). The two hand augers (A1–A2) indicate that the plastic silt (unit III) is underlain by medium sand (unit V), and a granule to pebble horizon (unit VI) at ~2–2.5 m depth (Figs. 3D and 4D; Appendix 1 [see footnote 1]).

Interpretation of Depositional History

The medium sand (unit V) and granule to pebble bed (unit VI) are coarser than the overlying stratigraphy and are consistent with deposits within the active floodplain of the Waimakariri River (Fig. 3D). Units V and VI are therefore

interpreted to most likely represent crevasse splay deposits from a pre-European flood event of the Waimakariri River (Brown and Weeber, 1992). The overlying plastic silt (unit III) was likely deposited in a marsh or oxbow lake adjacent to the meandering Avon River that periodically received sediment during flood events, as indicated by the interbedded lenses of fine to medium sand (unit IV). The normally graded beds of fine sand to silt (unit II, a–e) exposed in T1–T3 (Figs. 3, 4, and 5) are interpreted as overbank flood deposits from the nearby Avon River. The stratigraphy is consistent with the pre-European (i.e., pre–mid-nineteenth century) avulsion of the Avon River across the site and the historical reports of periodic flooding of the Avon River during periods of heavy rain between 1865 and 1953 (Cowie, 1957). Unit I is interpreted as a topsoil horizon. There are no well-documented rates of soil formation for the Christchurch region due to the varied land uses

throughout the development of the city, and so no surface age may be inferred from the topsoil thickness.

Radiocarbon dating of two subrounded wood fragments obtained from unit II in T3 at depths of 0.8 m (S1) and 0.9 m (S2) yielded ages of 2858–2493 B.C. (S1) and A.D. 1660–1803 (S2), respectively (Fig. 5; Table 1). Two small, subrounded wood fragments were also obtained from unit III in T1 from depths of 1.4 m (S3) and 1.55 m (S4). The samples yielded predominant ages of A.D. 1229–1276 (S3) and A.D. 665–765 (S4), respectively (Fig. 3B; Table 1). S1 yielded a complicated age spectra (Table 1) with a mean age significantly older than the bounding strata, suggesting that the dated material may be reworked detritus; therefore, it is excluded from further discussions. S2, S3, and S4 all were small, subrounded wood fragments that lacked root-like geometries or lateral continuity. We suggest that these ages approximate

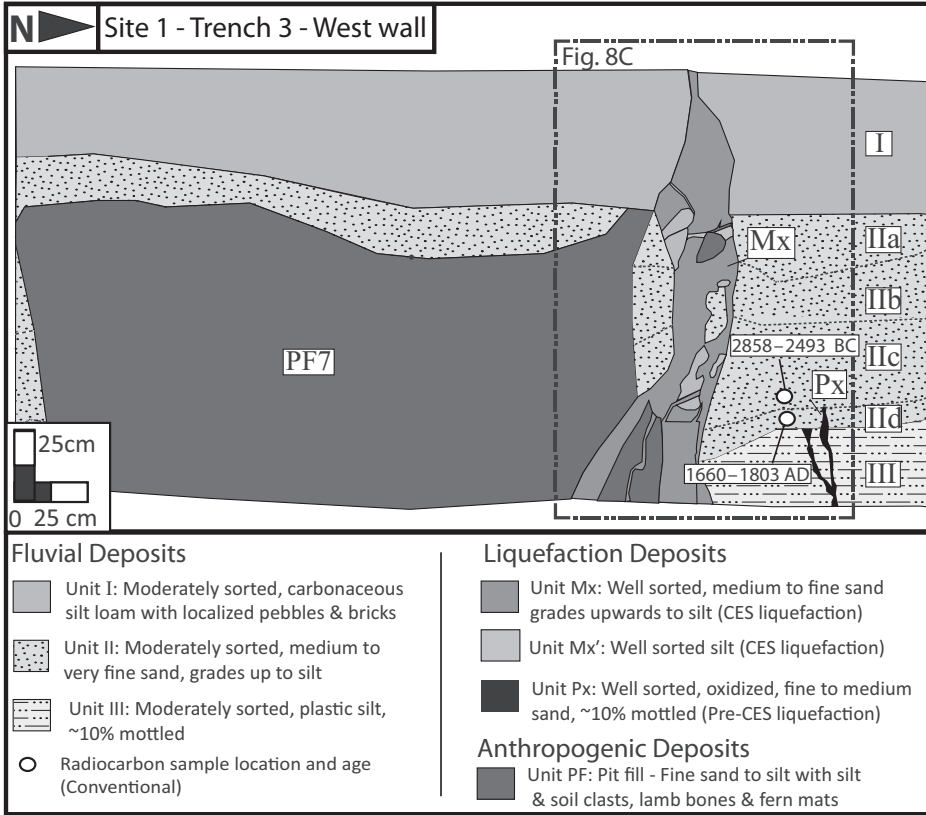


Figure 5. Detailed trench log of the west wall of T3. The Canterbury earthquake sequence (CES) liquefaction dike (Mx) crosscuts the fluvial (I–III) and anthropogenic (P7) stratigraphy from the trench floor to the surface. The pre-Canterbury earthquake sequence dike (Px) crosscuts the fluvial stratigraphy (I–III) from the trench floor to ~90–95 cm depth. The location and results of the ¹⁴C samples are also indicated.

the depositional age of the sediment due to the consistency between the reported ages of S2–S4. Therefore, the ages indicate that the trench stratigraphy was most likely deposited over a maximum period from ca. A.D. 665 to present.

OSL dating of two samples obtained from the unit II in T1 from depths of 0.86 m (O1) and 1.05 m (O2) yielded ages of 838 B.C. (±210 yr) and 818 B.C. (±210 yr), respectively (Fig. 3B; Table 2). During testing, it was observed from experimental data that these samples were composed of bleached and partially bleached sand and therefore were not sufficiently exposed to light prior to redeposition (N. Wang, 2013, personal commun.). These ages are interpreted to reflect maximum ages, with the depositional ages of the host sediment possibly much younger.

Trench Anthropogenic Stratigraphy

The fluvial stratigraphy exposed in T1–T3 is crosscut by anthropogenic pits, ~20–100 cm wide and ~20–90 cm deep, with subvertical walls (Figs. 3, 4, and 5). The pits contain silt (unit PF, for pit fill) with irregular lenses of car-

bonaceous silt (5%–10%), oxidized whole and fragmented lamb fetlock bones, fern mats, and fragments of ground-up and burnt bone (Fig. 6A; Appendix 1 [see footnote 1]). The lenses of burnt bone are surrounded by an oxidation front in unit III (Fig. 6D).

T1 (Fig. 3A) is crosscut by multiple anthropogenic pits (P1–P4, and P8). P1–P3 exhibit internal lensoidal stratigraphy and crosscut the fluvial stratigraphy from ~20 to ~70 cm depth to the trench floor. P4 (Fig. 3A) underlies and is separated from P3 by ~20 cm of unit II; it is composed of unit PF with rare fragments of oxidized bone and fern mat. A fifth pit (P8) was exposed as the west wall of T1 was cut back by ~50 cm; it contains unit PF with no internal lenses (Fig. 3C). Excavation of P3, P4, and P8 in plan view indicates that these pits comprise a corner of a larger pit (P9) that extends from ~20 cm to 1.8 m depth and is capped by an iron lid (Fig. 7). The intervening bed of unit II between P3 and 4 (Fig. 3A) was not observed during excavation of P9. It is possible that the relationship observed on the wall of T1 reflects an irregularly dug wall or collapse of the corners of the larger pit into

the surrounding fluvial sediment. T2 is crosscut by two pits (P5 and P6; Figs. 4 and 6A), and T3 is crosscut by one pit (P7; Fig. 5), all of which are composed of unit PF and exhibit internal lensoidal stratigraphy.

Interpretation of Anthropogenic History

A wool scouring factory operated adjacent to site 1, and historical photographs place the park within the property boundaries of the factory (Bremer, 1985). The history of the wool scouring industry within Avonside is poorly documented; however, it is known that the Avonside scour opened “shortly after” the Woolston scoury was established in A.D. 1864, with activity continuing at the site until ca. 1905 (Bremer, 1985). Cesspits are reported as being in use during production in an attempt to reduce pollution in the Avon River (Bremer, 1985). We interpret the anthropogenic pits identified in T1–T3 (Figs. 3, 4, 5, and 6A) as cesspits due to the irregular pit walls and internal stratigraphy consistent with intermittent shoveling of waste (Fig. 7). The presence of only fetlock bones further supports that these are cesspits, because fetlock bones were not removed during skinning and therefore would have been disposed of on site (Bremer, 1985). It is likely that the pits in T2 (P5–P6; Figs. 4 and 6A), T3 (P7; Fig. 5), and P1–P2 in T1 (Fig. 3A) also comprise sections of other large cesspits; however, this cannot be confirmed, as these pits were not excavated in plan view.

The anthropogenic pits crosscut the fluvial stratigraphy from ~20 cm depth, indicating that excavation of these pits postdated deposition of the fluvial stratigraphy beneath 20 cm. The recorded timing of production at the factory is consistent with a radiocarbon age of A.D. 1709–1932 obtained from a fern mat exposed in P8 (S5; Fig. 3C; Table 1). A charcoal fragment obtained within P9 at 1.8 m depth (S6) yielded a radiocarbon age of A.D. 1223–1279 (Fig. 7; Table 1). The reported age is inconsistent with the reported timing of production at the factory, suggesting that it may be derived from reworked detritus.

Canterbury Earthquake Sequence Liquefaction Features

Canterbury earthquake sequence liquefaction features were recognized in the subsurface by (1) their alignment with and traceable continuity into the observed surface Canterbury earthquake sequence sand blows and fissures and (2) their crosscutting relationship with the fluvial and anthropogenic stratigraphy. These liquefaction features were documented in detail in order to record the morphologies of subsurface liquefac-

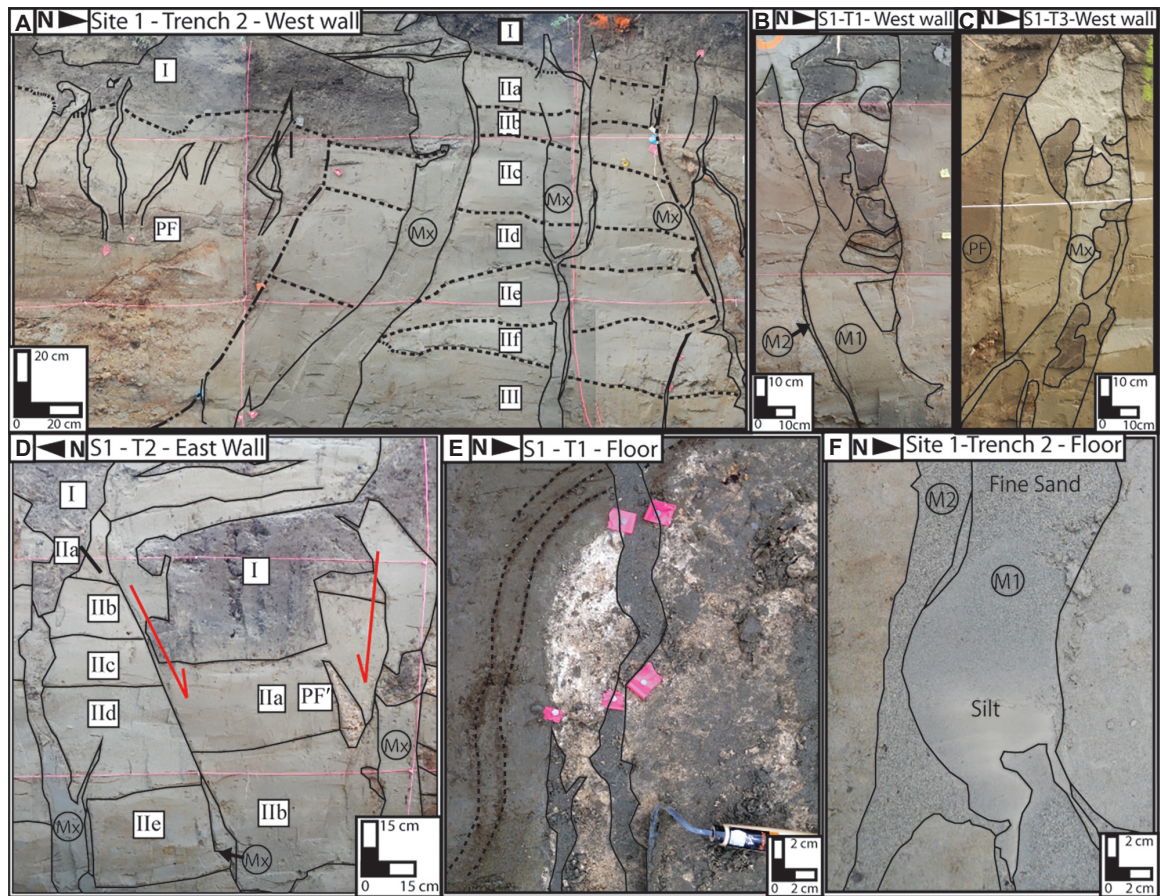


Figure 6. (A) Interpreted field photograph of the west wall of T2 (site 1). The fluvial stratigraphy (I–II and outlined in black dotted line) and anthropogenic cesspits (PF and outlined in black lines and dots) are crosscut by Canterbury earthquake sequence liquefaction features (Mx and outlined in black solid lines). (B) The ~25-cm-wide lateral spreading fissure at the north end of T1 contains downdropped topsoil clasts and a dike-parallel silt lining that separates two Canterbury earthquake sequence events (M1 and M2). (C) The ~25-cm-wide lateral spreading fissure at the north end of T3 contains downdropped clasts of topsoil and unit PF. (D) The ~50-cm-wide lateral spreading fissure on the east wall of T2 forms a graben that downdrops the fluvial stratigraphy (I–III) by ~40 cm and is bounded by liquefaction dikes (Mx). (E) The lens of white bone fragments on the floor of T1 is surrounded by an oxidation front (dotted black line) and is crosscut by Canterbury earthquake sequence dikes (outlined in black). (F) The ~7-cm-wide dike on the floor of T2 exhibits 1–2-mm-thick, dike-parallel silt lining and internal silt lining (outlined in black), suggesting that two Canterbury earthquake sequence events are preserved within the one dike (M1 and M2). M1 also exhibits intradike sorting fining from fine sand to silt.

tion and assist with the identification and interpretation of pre-Canterbury earthquake sequence liquefaction features. The Canterbury earthquake sequence liquefaction features all consist of gray, well-sorted, fine to medium sand, unless otherwise stated, and lack the oxidation and mottling developed in the surrounding stratigraphy.

Canterbury Earthquake Sequence Lateral Spreading Fissures

The large (>50 cm in width) lateral spreading fissure intersected in T1 and T2 (Fig. 2B) is bounded by inward-dipping fractures in the subsurface, forming a graben (Figs. 3A and 6C). The grabens in T1 (Fig. 3A) and on the east

wall of T2 (Figs. 4B and 6D) are bounded by two subvertical, planar dikes, ~2–10 cm wide, that downdrop the stratigraphy by ~30–40 cm. The fissure can be traced across the floor of T2, where the bounding dikes are composed of medium sand with granules to pebbles (5%–10%) of oxidized sandstone (Fig. 4C). The fissure aligns with an ~20-cm-wide, subvertical, planar dike on the west wall of T2 (Fig. 4A).

Canterbury Earthquake Sequence Liquefaction Dikes

The smaller lateral spreading fissure (<50 cm in width) intersected in T1 and T3 (Fig. 2B) corresponds with ~25-cm-wide, subvertical, planar

dikes in the subsurface that crosscut the fluvial and anthropogenic stratigraphy and feed into the surface fissure. The dikes decrease in width and fine upward (Figs. 3A, 6B, and 6C). The dike in T1 contains downdropped clasts of topsoil ~5–15 cm in diameter (Figs. 3A and 6B), while the dike in T3 contains incorporated clasts of topsoil and unit PF ~5–10 cm in diameter (Fig. 6C).

Smaller subvertical, planar dikes, ~2–10 cm wide in T1–T3, crosscut the stratigraphy from the trench floor to 10 cm depth, where they pinch out, and they are composed of fine sand to silt (Figs. 3A, 4A, 5, and 6A). Silt layers, ~1–2 mm thick, are observed along the dike margins (Fig. 6B) and internally within the dikes, where they

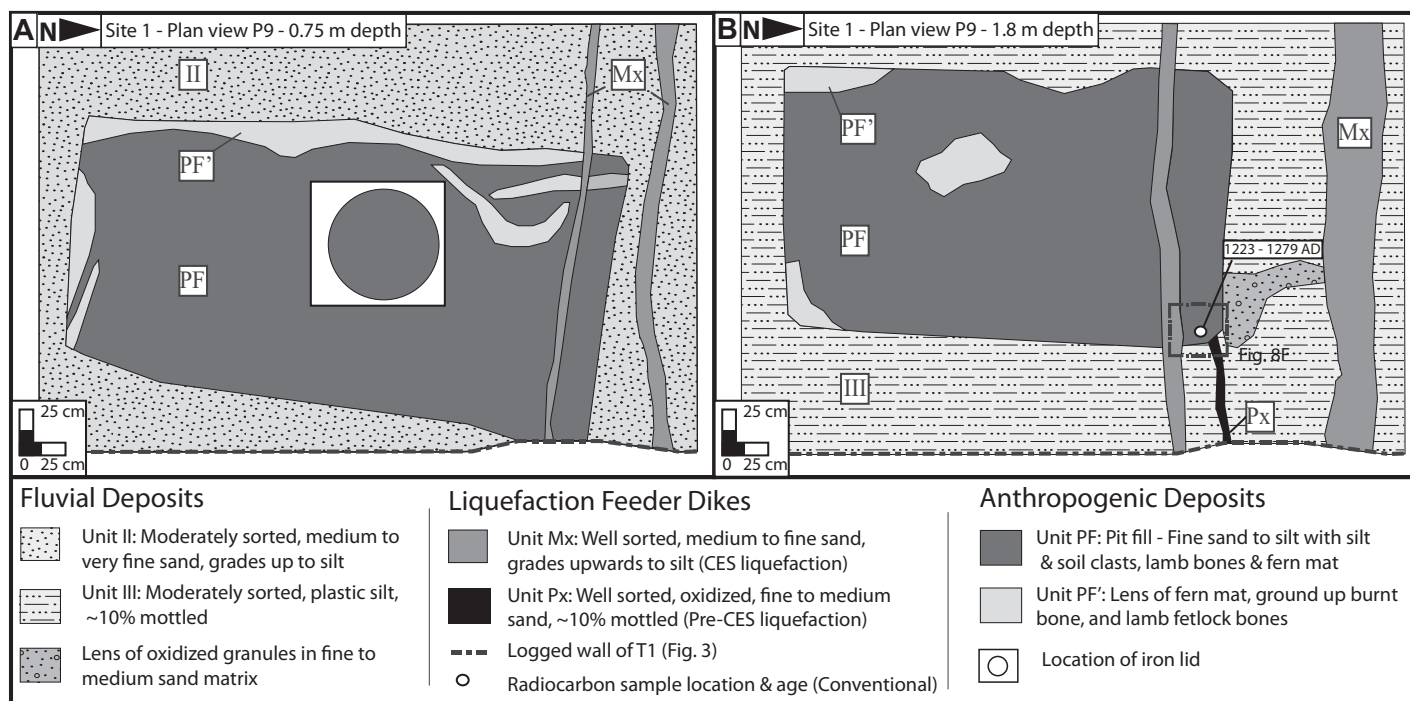


Figure 7. (A) Detailed log of the large pit (P9) as exposed in plan view at 0.75 m depth. The pit (PF) crosscuts the fluvial sand (unit II), is crosscut by a Canterbury earthquake sequence (CES) dike (Mx), and is capped by an iron lid (indicated). The location of the logged section of T1 (Fig. 3A) is also indicated. (B) Detailed log of the large pit (P9) as exposed in plan view at 1.8 m depth. The pit crosscuts the fluvial silt (unit III) and the pre-Canterbury earthquake sequence dike (Px), and it is crosscut by a Canterbury earthquake sequence dike.

separate two units of fine sand (Fig. 6F). Lateral grading from fine sand to silt is also observed within the ~5–10-cm-wide dike on the floor of T2 (Figs. 4C and 6F). Dikes ~1–2 cm wide and 10–40 cm long were observed to originate within the pit fill (unit PF) on the west wall of T2 (Figs. 4A and 6A). These small dikes terminate beneath the surface, are composed of silt, and increase in width with depth.

The dikes identified in T1–T3 crosscut the fluvial and anthropogenic stratigraphy from the trench floor to between 0–10 cm depth (Figs. 3, 4, and 5). This indicates that formation of these dikes postdated deposition of the lower (beneath 10 cm) stratigraphy. The dikes that reach the surface feed into the Canterbury earthquake sequence liquefaction fissures and sand blows (Figs. 3, 4, 5, and 6), confirming that they formed during the Canterbury earthquake sequence. The similar morphology, composition, and lack of mottling and oxidation of the dikes that pinch out beneath the surface indicate that they are also of Canterbury earthquake sequence age. A detrital wood fragment obtained from within an ~5-cm-wide dike at ~1.15 m depth in T1 yielded a radiocarbon age of 810–792 B.C. (S7; Fig. 3B; Table 1). This is interpreted to reflect the maximum depositional age of the liquefied sediment source.

Interpretation of Canterbury Earthquake Sequence Liquefaction Features

The alignment of the subsurface grabens and dikes with the surface fissures indicates that these features represent lateral spreading fissures in-filled by liquefied sediment. The increasing width of the dikes with depth suggests that these features formed by the upward injection of sediment, as opposed to downward-propagating surface cracking, in which features would be expected to decrease in width with depth (Figs. 3, 4A, 4B, and 5; Counts and Obermeier, 2012). Individual dikes range in width from ~2 to 50 cm (Fig. 3, 4, 5, and 6A). These varied widths likely reflect complexities in the three-dimensional dike geometries resulting from interactions with host sediment, variations in lateral spreading, and differing source depths.

The predominately gray, well-sorted, fine to medium sand comprising the <50-cm-wide Canterbury earthquake sequence dikes is consistent with the fine to medium sand of unit V identified in A1, suggesting that it may be sourced from this unit (Fig. 3D). The medium sand with localized granules of oxidized sandstone comprising the >50-cm-wide Canterbury earthquake sequence dike on the floor of T2 (Fig. 4C) is consistent with unit VI identified in A1 at 2.2–2.8 m depth (Figs. 3D and 4D). The

CPTu sounding (Figs. 2B and 9) indicates that the stratum from 1.5 to 2.2 m depth (unit V in A1; Fig. 3D) was potentially liquefiable under the ground accelerations generated in the 2010 Darfield, and 2011 Christchurch earthquakes ($FS > 1$). The underlying stratum from 2.2 to 2.8 m (unit VI) was not liquefiable during the Canterbury earthquake sequence; however, the unit at 2.8–3 m was potentially liquefiable in the February 2011 earthquake (Fig. 9). Therefore, the CPTu supports the interpretation that the smaller Canterbury earthquake sequence dikes were likely sourced from unit V, while the >50-cm-wide dike was likely sourced from the unit at 2.8–3 m depth, and likely entrained granules from unit VI during ejection. As the unit at 2.8–3 m was only liquefiable during the February event, the larger dike likely formed during this event. This indicates that the higher shaking intensities that occurred during the February 2011 event likely formed wider dikes (>50 cm) and triggered liquefaction at greater depths than the other Canterbury earthquake sequence events.

The well-sorted and fining-upward nature of the medium to fine sand to silt within the dikes indicates that sediment sorting occurred during ejection/injection. The sediment sorting is consistent with the Hjulström curve, in which very

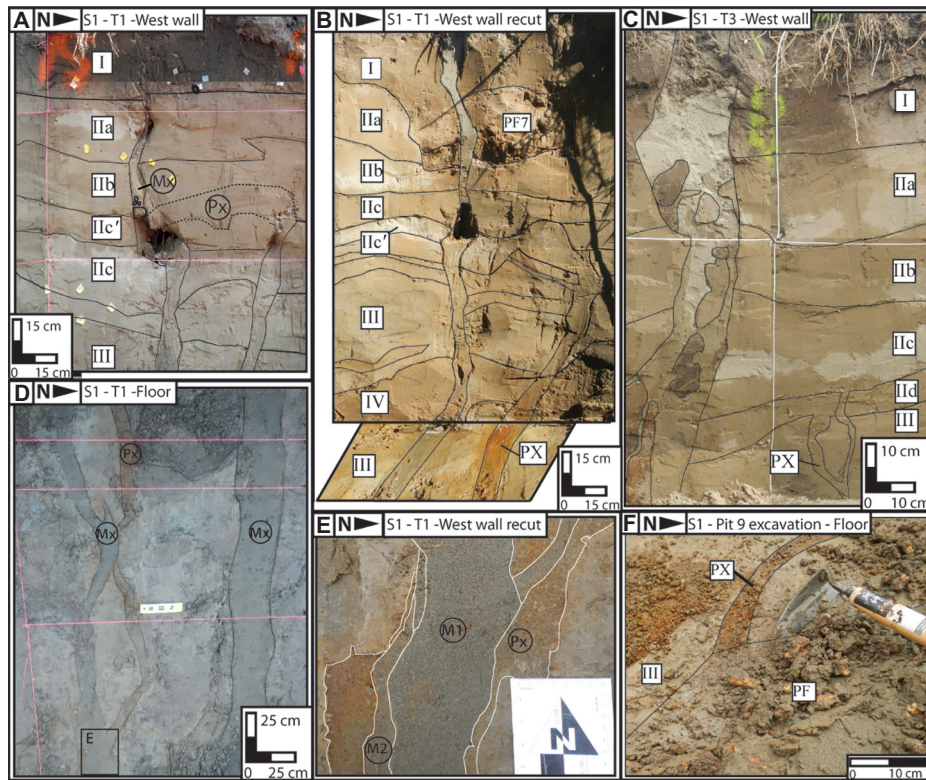


Figure 8. (A) Interpreted field photograph of the north end of T1, indicating the alignment of the Canterbury earthquake sequence (Mx) and pre-Canterbury earthquake sequence (Px) dikes. The Canterbury earthquake sequence dike (Mx) crosscuts the fluvial stratigraphy (I–III) and the pre-Canterbury earthquake sequence dike (Px). The pre-Canterbury earthquake sequence dike crosscuts the stratigraphy to ~70 cm. (B) Interpreted field photograph of the re-cut in the north wall of T1. The Canterbury earthquake sequence dike crosscuts the fluvial stratigraphy (I–III) and pre-Canterbury earthquake sequence liquefaction dike (PX). The pre-Canterbury earthquake sequence dike (PX) dissipates into the fluvial sand (unit IIc) at ~70 cm depth. (C) Interpreted field photograph of the north end of T3. The Canterbury earthquake sequence dike (Mx) crosscuts the fluvial stratigraphy (I–III) to the surface. The pre-Canterbury earthquake sequence dike (PX) crosscuts the fluvial silt (III) and dissipates into the fluvial sand (unit IIc) at ~90 cm depth. (D) The Canterbury earthquake sequence dike (Mx) also crosscuts the pre-Canterbury earthquake sequence dike (Px) on the floor of T1. (E) The Canterbury earthquake sequence dike (Mx) crosscuts the pre-Canterbury earthquake sequence dike on the floor of T1 and contains an internal, dike-parallel silt lining (outlined in white) that separates two Canterbury earthquake sequence liquefaction events (M1 and M2). (F) Excavation of P9 (PF) in plan view reveals that the pit crosscuts the pre-Canterbury earthquake sequence dike (Px) and fluvial silt (III).

fine sand has the lowest critical velocity required to entrain particles and thus is mobilized first (Hjulström, 1939). The fining-upward trend may reflect decreasing flow velocity of the escaping fluids, possibly due to the formation of wide conduits (i.e., the lateral spreading cracks), enabling fluid pressure dissipation and resulting in a decreased grain size entrained in the flow. The intradike lateral grading from fine sand to silt (Fig. 6F) indicates that flow rates varied laterally within the dike during ejection. This sorting may reflect obstruction of flow around an object (e.g., topsoil clast), resulting in the deposition of silt

in voids as the flow waned. The intradike clasts of topsoil and unit PF (Figs. 3A, 5, 6B, and 6C) likely formed by fragmentation of the host sediment during sediment ejection, with the clasts settling through the liquefied sediment as the flow waned or as a result of their higher density compared to the surrounding liquefied sediment.

The dike-parallel silt linings on the dike margins (Figs. 6B and 6F) suggest that flow velocities were lower on the dike margins, resulting in silt being deposited out of suspension. The preservation of dike-parallel silt linings within a dike (Figs. 6B and 6F) suggests that multiple

liquefaction episodes may be preserved within one dike. This may reflect either pulsed ejection of sediment during one earthquake, or conduit reactivation in successive Canterbury earthquake sequence events.

Pre-Canterbury Earthquake Sequence Liquefaction Features

Pre-Canterbury earthquake sequence liquefaction was identified in the trenches based on their structural similarities to/and crosscutting relationships with the Canterbury earthquake sequence liquefaction features and the surrounding stratigraphy.

Pre-Canterbury Earthquake Sequence Liquefaction Dike

The lateral spreading fissure intersected in T1 (Figs. 3A and 3B) and T3 (Fig. 5) crosscuts oxidized dikes on the trench wall and floor (Fig. 8). The oxidized dikes consist of well-sorted, oxidized, and mottled (~1–7 mm wide), medium sand with granules of oxidized sandstone (Fig. 8).

In T1, the ~7-cm-wide oxidized dike crosscuts unit III and unit IIc to ~70 cm depth, where it appears to dissipate and become indistinguishable from unit IIc (Figs. 3B and 8A). No deformation or evidence for the oxidized dike was observed in the overlying stratigraphy (Figs. 3B and 8A). The west wall of T1 was cut back by ~50 cm to further analyze this relationship (Fig. 3C). The oxidized dike continued to be traceable to ~70 cm depth, where it dissipates into the fluvial sand to silt of unit IIc (Figs. 3C and 8B). In T3, the oxidized dike crosscuts units III and IIc to ~90–95 cm depth (Figs. 5 and 8C), and is comparatively narrower (~2–3 cm wide) than in T1. Excavation of P9 in plan view revealed an oxidized dike that is crosscut by the pit at ~1.8 m depth (Figs. 7B and 8B). The oxidized dike emerges from the northwest side of P9, where it varies from ~2 to 4 cm in width.

Interpretation of Feature

The oxidized dikes identified in T1 (Figs. 3A and 3B) and T3 (Fig. 5) approximately align with the Canterbury earthquake sequence lateral spreading feature and exhibit similar subvertical and planar morphologies to the Canterbury earthquake sequence dikes, thus suggesting that the dikes were seismically triggered. The mottling within the oxidized dikes (Fig. 8) formed through precipitation of reduced iron in pore spaces during water-table lowering (Van Breemen and Buurman, 2002). The well-developed mottles in the oxidized dikes suggest long residence in fluctuating water tables, therefore suggesting that the dikes were emplaced in

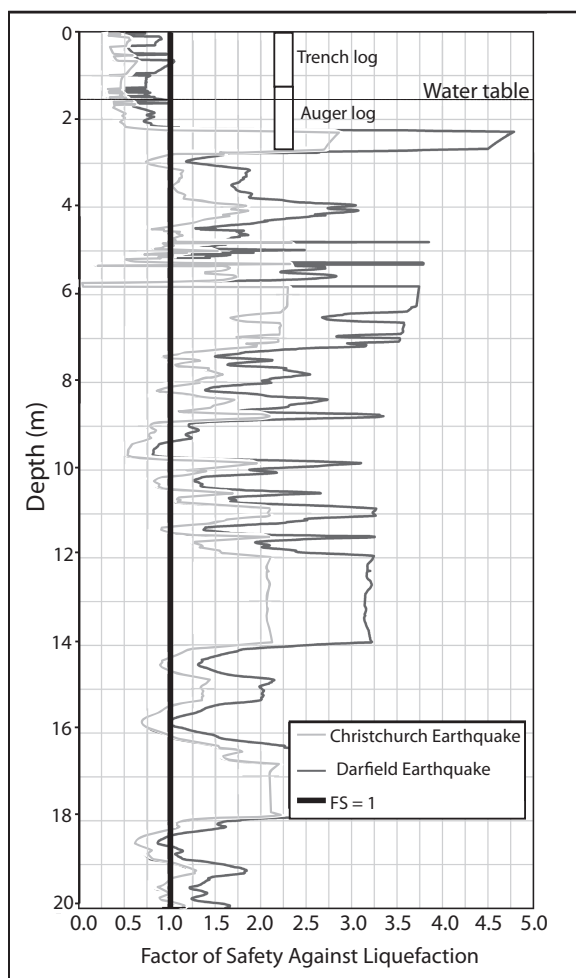


Figure 9. The CPTu (cone penetration test with pore-pressure [piezocone] measurement) test conducted at site 1 indicates that the sediment from 1.6 to 2.5 m depth was potentially liquefiable ($FS < 1$) under the peak ground accelerations (PGAs) generated in the September 2010 and February 2011 earthquakes. The sediment from 2.8 to 3 m depth was also potentially liquefiable ($FS < 1$) under the PGAs of the February 2011 earthquake (modified from Bastin et al., 2013).

an event predating the Canterbury earthquake sequence. To the best of our knowledge, there is no empirical data constraining the rate of mottle formation in a subsurface deposit under fluctuating water tables, so no absolute age for dike emplacement can be determined from the degree of mottling alone.

The pre-Canterbury earthquake sequence dike in T1 crosscuts units III and IId and is overlain by unit IIc (Fig. 3B), indicating that it most likely postdates deposition of units III and IId, and the A.D. 665–765 radiocarbon age for unit III (S4; Table 1). The pre-Canterbury earthquake sequence dike in T3 crosscuts units III and IId (Fig. 5), indicating that it postdates the radiocarbon age of A.D. 1660–1803 (S2; Table 1) derived from a charcoal sample in unit IId. These ages are considered to reflect maximum depositional ages, and the actual age of the pre-Canterbury earthquake sequence dikes may in fact be younger. The pre-Canterbury earthquake sequence dike crosscut by the cesspit (P9; Fig. 7B) indicates that dike injection must predate excavation of the cesspit. The exact age of the pit cannot be determined from historical

records; however, it most likely predates closure of the factory at ca. 1905.

The oxidized dikes can be traced between T1, T3, and adjacent to P9, where they continuously align with the ~25-cm-wide lateral spreading fissure. The traceability of these oxidized dikes suggests that they may comprise a prior lateral spreading fissure formed during a pre-Canterbury earthquake sequence earthquake event. The oxidized dikes decrease in width from ~7 cm in T1 (Fig. 3) to ~2–3 cm in T3 (Fig. 5) and adjacent to P9 (Fig. 7). This may reflect either varied widths along the length of the fissure and/or pinching out at the terminus of the fissure. The oxidized dikes in T1 and T3 exhibit similar morphologies to the ~25-cm-wide Canterbury earthquake sequence lateral spreading fissure, and they appear to dissipate into the fluvial sand to silt (unit II) with no obvious evidence for surface ejecta (Figs. 3B, 3C, and 5). It is possible that either the oxidized dikes reached the surface, with the ejecta being reworked during deposition of unit II (Figs. 3B and 8B), or the pre-Canterbury earthquake sequence dikes dissipated within a low-strength layer at depth.

Nonseismic methods for triggering liquefaction that are outlined in Owen and Moretti (2011), including gravity acting on slopes, unequal loading due to topography, density contrasts, fluid shear, and biological action, do not fit the depositional and hydrological setting of Avonside. The dike morphologies also do not correspond with the non-seismic soft-sediment deformation features outlined in Montenat et al. (2007) and Counts and Obermeier (2012), further supporting the interpretation that the oxidized dikes were seismically triggered.

The medium sand with localized granules of oxidized sandstone composition of the pre-Canterbury earthquake sequence dikes (Figs. 3, 5, and 8) is consistent with the Canterbury earthquake sequence dike on the floor of T2 (Fig. 4C) and unit VI at 2–2.6 m depth (Figs. 3D and 4D). The consistent composition suggests that both the pre-Canterbury earthquake sequence and Canterbury earthquake sequence dikes entrained material from this unit and may have been sourced from the underlying unit at 2.8–3 m depth, which was potentially liquefiable ($FS > 1$) in the February 2011 earthquake (Fig. 9).

SITE 2: BRACKEN STREET

The Bracken Street site has flat topography with elevations of 0.6–0.8 m above sea level across the site (Fig. 2). The dwelling on the site was erected in ca. A.D. 1910. A trench (T4) was excavated perpendicular to the aligned sand blow vents (Fig. 2C), to a length of ~10 m and a depth of ~1.4 m. The depth of the trench was limited by the depth to the water table, which was ~1.3–1.4 m during excavation.

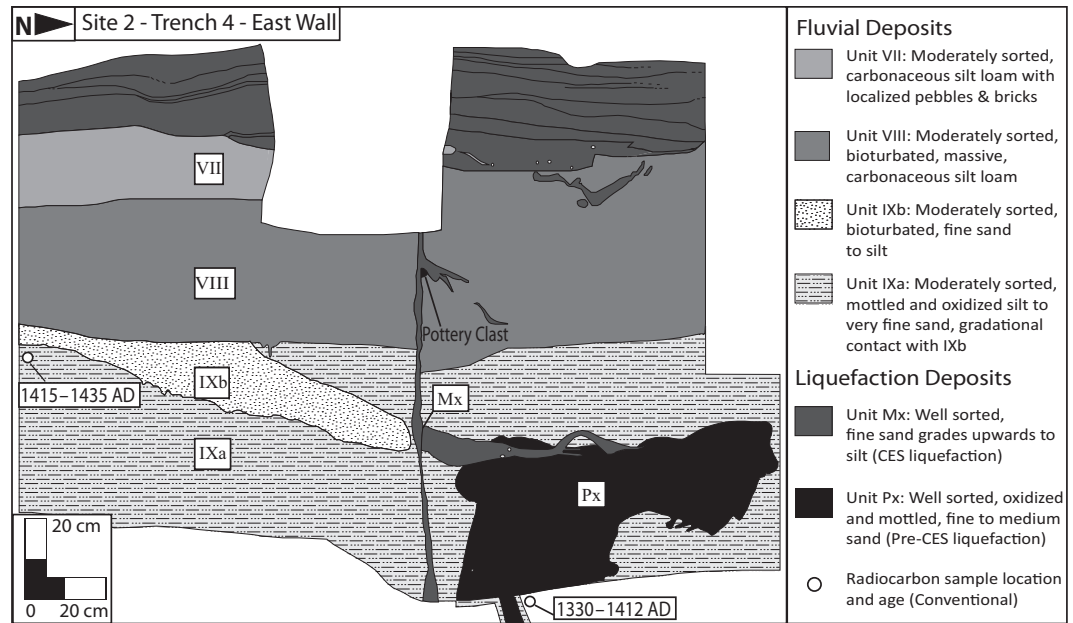
Trench Fluvial Stratigraphy

T4 exposed stratigraphy composed of nonplastic silts (unit IXa) with interbedded, lenticular, very fine sand (unit IXb), capped by ~50 cm of topsoil (unit VIII; Fig. 10; Appendix 1 [see footnote 1]). The upper ~25 cm section of topsoil contains a discontinuous anthropogenic layer of pottery, glass, and pebbles (unit VII; Fig. 10).

Interpretation of Depositional History of the Site

The nonplastic silts (unit IXa) exposed in T4 (Fig. 10) are interpreted as overbank flood deposits from the Avon River in a low-energy depositional setting such as that of a marsh or oxbow lake. The interbedded lenses of very fine sand (unit IXb) indicate that the area was periodically flooded by higher-energy events. The lenticular morphology of these fine sand lenses (unit IXb) indicates that the flood events sometimes formed small channels. The exposed stra-

Figure 10. Detailed trench log of the south end of the east wall in T4 (site 2). The Canterbury earthquake sequence (CES) dike (Mx) crosscuts the fluvial stratigraphy (VII–IXa) and the dike-fed, pre-Canterbury earthquake sequence injection feature (Px), and it feeds into the surface ejecta. The stratigraphy within the surface ejecta, and the location and ¹⁴C ages of the samples are also indicated.



tigraphy reflects the present depositional setting of the site within the low-elevation (1–1.5 m above sea level) floodplain of the Avon River (Fig. 2) and is consistent with historical reports of periodic flooding of the Avon River during periods of heavy rain (Cowie, 1957).

Radiocarbon dating of two detrital wood fragments obtained from unit IXa at depths of 0.5 m (S8) and 1.1 m (S9) yielded ages of A.D. 1415–1435 (S8) and A.D. 1330–1412 (S9), respectively (Fig. 10; Table 1). These ¹⁴C ages indicate that the stratigraphy was deposited over a maximum period from A.D. 1330 to present.

Canterbury Earthquake Sequence Liquefaction Features

Canterbury earthquake sequence liquefaction features were recognized in T4 (Fig. 10) by their traceable continuity into the observed surface sand blows. The Canterbury earthquake sequence features were documented in detail to determine whether the morphologies of liquefaction features were consistent between the two sites, and to aid identification of pre-Canterbury earthquake sequence liquefaction features. The Canterbury earthquake sequence liquefaction features are all composed of gray, well-sorted, fine sand to silt unless otherwise stated.

Canterbury Earthquake Sequence Liquefaction Dikes

The linear array of surface sand blows intersected at the southern end of T4 (Fig. 2D) aligns with an ~4–5-cm-wide, subvertical, planar dike in the subsurface that crosscuts the fluvial stratigraphy from the trench floor to the surface

(Fig. 10). Thinner, subvertical, planar dikes, ~0.5–2 cm wide, that crosscut the stratigraphy from the trench floor to ~10 cm depth are evident at the northern end of the trench.

The dikes all increase in width with depth and lack the oxidation and mottling developed in the surrounding stratigraphy (Fig. 10). No evidence for vertical grading is observed within these dikes. Contact-parallel silt linings, ~1 mm thick, are observed on the margins of the ~4–5-cm-wide dikes (Fig. 10), while no silt lining is observed on the margins of the ~0.5–2-cm-wide dikes.

Canterbury Earthquake Sequence Subsurface Liquefaction Sill

The ~4–5-cm-wide dike crosscuts an ~2-cm-wide sill at ~50 cm depth (Fig. 10). The sill exhibits a composition consistent with that of the Canterbury earthquake sequence dike and is separated from the dike by the ~1–2-mm-thick dike-parallel silt lining (Fig. 10).

Interpretation of Canterbury Earthquake Sequence Liquefaction Features

The ~4–5-cm-wide dike crosscuts the fluvial stratigraphy from the trench floor to the surface (Fig. 10), indicating that it postdates deposition of the fluvial stratigraphy. The alignment of the subsurface dike with the surface sand blow (Fig. 10) confirms that it formed during the Canterbury earthquake sequence, which is further supported by its lack of oxidation and mottling. The sill and the ~0.5–2-cm-wide dikes are of similar composition to the Canterbury earthquake sequence dikes that unequivocally reach the surface and also lack oxidation and mottling. The similar composition indicates that the smaller

dikes and sill also formed during the Canterbury earthquake sequence. The increasing width of the dikes with depth (Fig. 10) supports the interpretation of these dikes as having formed by the upward injection of sediment (Counts and Obermeier, 2012). The subvertical and planar morphology of the dikes at site 2 is consistent with the morphologies of the dikes documented at site 1. The consistent morphology indicates that dike geometries, as well as the well-sorted grain-size distributions, may be used to identify liquefaction features in the subsurface and in the absence of surface ejecta.

The dike-parallel silt linings along the margin of the ~4–5-cm-wide dike (Fig. 10) indicate that flow velocities were lower adjacent to the dike wall. The presence of the silt lining separating the sill from the dike suggests that the sill formed prior to the last liquefaction event ejected through the dike. This indicates that at least two generations of Canterbury earthquake sequence liquefaction are preserved within the subsurface.

The dikes at site 2 (Fig. 10) are comparatively narrower than those identified at site 1 (~5 cm at site 2 and up to 25 cm at site 1; Figs. 3, 4, 5, and 10). The varied widths may be attributed to the varied distance of each site from the river, as it was observed that the width and spatial density of surface features decrease away from the river (Bastin et al., 2013). The varied widths of the dikes may also reflect variations in the stratigraphy overlying the liquefied layers, which are predominantly composed of fluvial silts at site 2 and fluvial sands at site 1. It is possible that the predominately silt stratigraphy at site 2 may inhibit fracturing, thus possibly resulting in the formation of comparatively narrower dikes.

Pre-Canterbury Earthquake Sequence Liquefaction Features

Pre-Canterbury earthquake sequence liquefaction features were identified in T4 based on their structural similarities and crosscutting relationships with the Canterbury earthquake sequence liquefaction features and the surrounding stratigraphy, and from comparison with the pre-Canterbury earthquake sequence features identified at site 1.

The Canterbury earthquake sequence dike at the southeast end of T4 crosscuts a bulbous-shaped lens of oxidized and mottled, well-sorted, fine to very fine sand (Fig. 10). This lens crosscuts the fluvial stratigraphy from the trench floor to ~80 cm depth and exhibits irregular and bioturbated contacts (Fig. 10). Excavation around this feature revealed a dike at ~1.5–1.7 m depth that merges with the bulbous lens and is of consistent grain size and sorting (Fig. 10). The dike ranges from 5 to 7 cm in width and exhibits a similar subvertical, planar geometry to the Canterbury earthquake sequence dike at site 2 (Fig. 10), and the oxidized dikes at site 1 (Fig. 8). Excavation beyond this point was limited by the height of the water table.

Interpretation of Pre-Canterbury Earthquake Sequence Liquefaction Features

The dike beneath the oxidized lens (Fig. 10) indicates that it formed by the upward injection of liquefied sediment. The similar subvertical, planar geometry of the oxidized dike and the adjacent Canterbury earthquake sequence dike indicates that the oxidized feature was seismically triggered. The oxidation and mottling within this feature indicate that it has been subjected to prolonged fluctuations in the height of the water table, indicating that it predates the Canterbury earthquake sequence. The bulbous shape of the oxidized lens, combined with its irregular contacts (Fig. 10) and lack of evidence for surface ejecta, suggests that this feature formed by the subsurface injection of liquefied sediment. The bulbous morphology of this feature is inconsistent with the Canterbury earthquake sequence injection sills observed at both sites 1 and 2. Therefore, we suggest that this feature may reflect injection into and subsequent deformation of a lens of fine sand, possibly being the paleochannel comprising unit IXb (Fig. 10). Liquefaction dikes are likely to preferentially form within loosely consolidated sands such as that within a paleochannel, as the sand provides a path of lower resistance compared to the surrounding silt. The site-specific depositional and hydrological conditions and the bulbous morphology of the oxidized feature are inconsistent with the liquefaction-triggering

mechanisms and morphologies of nonseismic liquefaction features described in Montenat et al. (2007), Owen and Moretti (2011), and Counts and Obermeier (2012). This supports the interpretation that this oxidized lens and associated dike formed during a pre-Canterbury earthquake sequence earthquake.

The pre-Canterbury earthquake sequence liquefaction injection feature crosscuts the fluvial silt (unit IXa) from the trench floor to ~80 cm depth. This indicates that this liquefaction feature likely formed in an event that postdated deposition of the fluvial silt (unit IXa), and the ¹⁴C ages of A.D. 1415–1435 (S8; Fig. 10; Table 1). The lack of surface ejecta associated with this feature indicates that the causative earthquake triggered liquefaction at depth; however, it did not generate the shaking intensities required to fracture the overlying soil cap and eject liquefied sediment to the surface at this location. It is possible that localized ejecta did form at other locations across this site and were not intersected within this trench. The lack of surface ejecta means that the ground surface at the time of injection cannot be determined, and no additional constraints can be placed on the timing of the paleoearthquake. The depth of the liquefied source stratum for the Canterbury earthquake sequence dikes and pre-Canterbury earthquake sequence liquefaction feature cannot be determined for this site because excavation was limited by the shallow water table.

POSSIBLE TIMING AND SEISMIC SOURCE FOR THE PALEOLIQUEFACTION

Timing and Origin of Paleearthquake(s)

The approximate timing of the earthquake(s) forming the pre-Canterbury earthquake sequence liquefaction features at sites 1 and 2 can be approximated by combining crosscutting relationships with ¹⁴C ages of the host sediments. The pre-Canterbury earthquake sequence dikes at site 1 crosscut the strata to ~70 cm depth in T1 (Fig. 3) and ~90–95 cm depth in T3 (Fig. 5) and are crosscut by P9 (Figs. 7 and 8B). This indicates that the pre-Canterbury earthquake sequence dikes postdate the depositional age of A.D. 1660–1803 for unit IIc (S2; Fig. 5; Table 1) and predate the closure of the wool scouring factory in ca. 1905.

The OSL ages (Fig. 3B; Table 2) are within error of the ¹⁴C age of 810–792 B.C. for the liquefied source strata (Table 1). It is possible that the OSL ages are dominated by reworked sediment sourced from the liquefied unit or its age equivalent elsewhere via redeposition of liquefied material ejected from depth, bioturba-

TABLE 3. INFERRED MAGNITUDES AND MMI VALUES FOR THE FIVE HISTORIC EARTHQUAKES WITH THE 50TH PERCENTILE PEAK GROUND ACCELERATION (PGA), AND CALCULATED 16TH, 50TH, AND 84TH PERCENTILE PGA_{7.5} VALUES FOR SITE 1

Event	M _w	MMI	Approx. distance from epicenter (km)	PGA 50th perc.	PGA _{7.5} 16th perc.	PGA _{7.5} 50th perc.	PGA _{7.5} 84th perc.	Calculated MMI
1869 Christchurch	4.8 ± 0.1	7 ¹	4	0.148 ± 0.013	0.040 ± 0.005	0.074 ± 0.009	0.124 ± 0.005	7
1870 Lake Ellesmere	5.7 ± 0.1	6 ¹	37	0.049 ± 0.004	0.017 ± 0.002	0.031 ± 0.003	0.055 ± 0.005	5.5
1888 Hope fault	7.2 ± 0.1	6 ²	102	0.046 ± 0.0035	0.026 ± 0.002	0.043 ± 0.004	0.071 ± 0.0017	5
1901 Cheviot	6.8 ± 0.1	6–7 ³	105	0.034 ± 0.001	0.017 ± 0.001	0.028 ± 0.001	0.047 ± 0.001	4.5
1922 Motunau	6.4 ± 0.1	6–7 ³	58	0.042 ± 0.001	0.021 ± 0.001	0.036 ± 0.001	0.062 ± 0.001	5

Note: Source: 1—Downes and Yetton (2012); 2—Cowan (1991); 3—Stirling et al. (1999). M_w—moment magnitude; MMI—modified Mercalli intensity; perc—percentile.

tion causing mixing of the surface ejecta with the surrounding fluvial deposits, or via erosion and redeposition of ca. 2.6–2.8 ka sediment from elsewhere without bleaching.

The pre-Canterbury earthquake sequence liquefaction feature at site 2 crosscuts the fluvial stratigraphy to ~80 cm depth (Fig. 10), indicating that it postdates the depositional age of A.D. 1415–1435 for unit IXa. No additional constraints on the timing of the earthquake can be concluded from crosscutting relationships; therefore, it cannot be concluded whether the pre-Canterbury earthquake sequence liquefaction features at both sites formed during the same earthquake event.

The historic record of earthquakes within the wider Christchurch area is limited to post-1843, following European settlement. Historic reports indicate that five damaging earthquakes occurred within ~150 km of Christchurch between 1869 and 1922 (Fig. 1B; Pettinga et al., 2001; Downes and Yetton, 2012). The magnitudes and inferred Modified Mercalli Indices (MMI) in Christchurch for each of these events are presented in Table 3 (Downes and Yetton, 2012). The 1869 M_w ~4.8 Christchurch earthquake occurred on 5 June 1869 at NZST 8.30 a.m. and was felt throughout the city (Elder et al., 1991; Stirling et al., 1999; Pettinga et al., 2001; Downes and Yetton, 2012). The highest shaking intensity was recorded within the Central Business District (CBD) causing the collapse of chimneys, the Christchurch cathedral spire, and a brick wall of a house (Stirling et al., 1999). Damage within Avonside and northeast Christchurch included extensive damage to the contents of residential properties, and many damaged or fallen chimneys. The reported damage corresponds with the effects of a MMI 7 earthquake (Downes and Yetton, 2012). Downes and Yetton (2012) assigned a macroseismic epicenter of 43.55°S, 172.60°E and upper-crustal hypocentral depth of 5 km, which is located at the center of the isoseismal pattern based on the accounts from residents and the distribution of damage (Stirling et al., 1999). Following the earthquake, it was observed by a local resident that “the tide runs higher up the Heathcote River than formerly,” suggesting that settlement, potentially induced by liquefaction, may have occurred (Downes and Yetton, 2012).

Damage during the 1870 ~ M_w 5.7 Lake Ellesmere earthquake was less widespread, with only damage to the contents of residential properties and chimneys reported within Avonside. The 1888 ~ M_w 7.2 North Canterbury and 1901 ~ M_w 6.8 Cheviot earthquakes caused widespread damage within the wider Christchurch area, including toppling of the Cathedral spire during

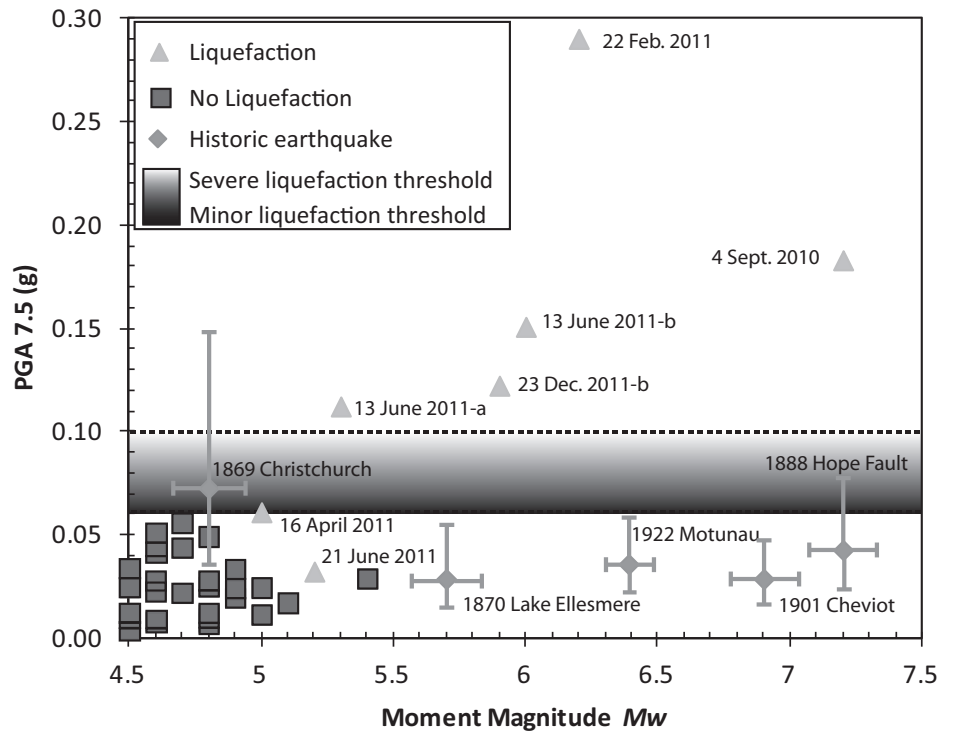


Figure 11. The calculated $PGA_{7.5}$ (peak ground acceleration equivalent for a M_w 7.5 event) for the Canterbury earthquake sequence events that did and did not cause liquefaction at site 2 compared with earthquake magnitude (M_w). The calculated median $PGA_{7.5}$ (box) and associated 16th and 84th percentiles (error bars), and inferred magnitudes for the paleo-events are also plotted. The plotted $PGA_{7.5}$ values are compared to the liquefaction triggering thresholds for minor to severe liquefaction during the Canterbury earthquake sequence as constrained for site 2 by Quigley et al. (2013).

both events (Cowan, 1991; Downes and Yetton, 2012). Damage was also reported in Christchurch following the 1922 ~ M_w 6.4 Motunau, North Canterbury, earthquake (Downes and Yetton, 2012). No surface manifestation of liquefaction was reported in Avonside following any of these events; however, it is possible that localized surface ejecta formed and went unreported due to the sparsely populated, rural and industrial nature of much of this area at this time. Large known prehistoric earthquakes prior to the settlement of Christchurch during the time interval encompassing the pre-Canterbury earthquake sequence liquefaction features include the 1717 Alpine fault M_w ≥ 7.9 (Sutherland et al., 2007) and ca. 500–600 yr B.P. M_w ≥ 7.1 Porters Pass fault earthquakes (Howard et al., 2005). The approximate epicentral locations and shaking intensities generated in Christchurch for these events are poorly constrained given the broad constraints on earthquake M_w and the lack of historical accounts. Additional large earthquakes in the Canterbury region are not considered due to the limited historical record.

Triggering of Liquefaction

The $PGA_{7.5}$ 0.06g liquefaction-initiation threshold at site 2 (Quigley et al., 2013) was established based on the observation of localized, small sand blows (~20 cm in diameter) that formed in the M_w 5.0 April 2011 earthquake. Widespread liquefaction ejecta were reported at the site at $PGA_{7.5} > 0.1g$ (Fig. 11). No empirically derived liquefaction triggering threshold was established for site 1; however, a similar threshold is likely given their geographic proximity, the similar geomorphic and geologic settings, and the similar water-table depths.

Site-specific $PGA_{7.5}$ estimates were derived for site 1 for the five well-documented historical events using the ground motion prediction equation (GMPE) outlined by Bradley (2013; Table 3). Site class E (very soft soil) characteristics were assumed for the study site. This GMPE is a New Zealand-specific model derived from comparison of four different preexisting models and calibrated against recorded ground motions in New Zealand (Bradley, 2013). The model utilizes the inferred magnitude, distance from epicenter, predominant rock type, and fault type

(i.e., normal, reverse, or strike slip) to calculate the approximate PGA experienced at the site (Table 3). Directionality was not considered due to the lack of constraints on the rupture directivity. The results provide a distribution with both the median and standard deviation PGAs. The 16th and 84th percentiles of this distribution were derived from the 50th percentile median PGA (Table 3). The PGA values were M_w 7.5-weighted ($PGA_{7.5}$) using the methodology outlined in Idriss and Boulanger (2008). The $PGA_{7.5}$ value enables direct comparison of ground accelerations generated by events with different M_w and epicentral distances. Here, we plot the median $PGA_{7.5}$ and 16th and 84th percentiles as error bars (Fig. 11), and compare the plotted $PGA_{7.5}$ for each event with the liquefaction triggering thresholds of $PGA_{7.5} \sim 0.06g$ for minor liquefaction and $PGA_{7.5} 0.1g$ for severe liquefaction at site 2 (Fig. 11). Of the five historical events, only the 1869 Christchurch earthquake produces a modeled median (50th percentile) $PGA_{7.5}$ that exceeds the threshold for minor liquefaction (Table 3). The 1869 earthquake predates closure of the wool scouring factory; therefore, it is possible that the pre-Canterbury earthquake sequence dikes at site 1 formed during this event, and the pit (P9) was excavated following this event.

Liquefaction during the Canterbury earthquake sequence was reported at distances of ~ 8 km from the epicenter following the 19 October 2010 M_w 5.0 aftershock (Cubrinovski and Green, 2010) and ~ 14 km from the epicenter of the 16 April 2011 M_w 5.0 aftershock (Quigley et al., 2013). This indicates that moderate-to-large (M 5–7.9) events can trigger liquefaction at distances greater than that predicted from empirical global compilations of M_w versus “distance to most distal liquefaction feature” (Ambraseys, 1988; Galli, 2000; Cubrinovski and Green, 2010), particularly in highly susceptible sediments or in areas prone to seismic amplification. Therefore, it is possible that the 1869 earthquake triggered minor liquefaction at an approximate epicentral distance of 6 km in highly susceptible sediments. The termination of the pre-Canterbury earthquake sequence dikes at ~ 70 and ~ 90 cm depth indicates that either ~ 90 cm of sedimentation occurred at the site following the event, or that the dikes terminated beneath the surface. It is considered unlikely that ~ 90 cm of sediment accumulated at the site post-1869 and during production at the wool scouring factory, thus suggesting the dikes terminated at depth. However, the similar geometries of the pre-Canterbury earthquake sequence dikes and Canterbury earthquake sequence lateral spreading fissure suggest that the pre-Canterbury earthquake sequence dikes may comprise a lateral spread-

ing fissure. The geometry of the dikes, combined with the inferred sedimentation at the site, suggests that the pre-Canterbury earthquake sequence features formed in an event prior to the 1869 event. It is possible that these features formed during a large, far-field earthquake such as the $\sim M_w$ 7.9 \pm 0.3 1717 Alpine fault event, which postdates the depositional age of A.D. 1660–1803 for unit IIc (S2; Fig. 5; Table 1). The GMPE indicates that this event likely generated $PGA_{7.5}$, exceeding the liquefaction triggering threshold at the site (Bradley, 2013).

The New Zealand Seismic Hazard Model (NZSHM) predicts approximate return times of ~ 50 yr for PGAs of 0.11g (MMI 6–7) and ~ 200 yr for PGAs of 0.22g (MMI 7–8) for class C material (shallow soils) in the Christchurch area (Stirling et al., 2008). This suggests a high likelihood of earthquake-induced strong ground motions exceeding the liquefaction triggering threshold within the last ~ 220 yr, particularly in sediments that are highly susceptible to liquefaction (e.g., site class E, very soft soils; NZS 1170.5, 2004). The approximate return times exclude the occurrence of earthquake clustering and are therefore considered to reflect average return times.

Liquefaction Susceptibility of Avonside

The liquefaction potential of the two sites in Avonside is governed by their hydrologic, geologic, and geomorphic setting. The liquefaction potential of the subsurface sediments generally decreases over time due to sedimentation, compaction, and the formation of secondary cements (Seed and Idriss, 1982; Idriss and Boulanger, 2008). The water table within Avonside is tidally influenced and controlled by the height of the Avon River, which remains approximately at sea level. Therefore, subsurface sediments at ≥ 1 –2 m depth are likely to have remained in the saturation zone following initial deposition, which, combined with their relatively young age (810–792 B.C.; S7; Table 1), suggests that limited cementation or aging is likely to have occurred. Quigley et al. (2013) showed a power-law relationship between the spatial extent and maximum stratigraphic thicknesses of sediment ejecta during the Canterbury earthquake sequence with $PGA_{7.5}$. This implies that any changes to the liquefaction source sediment during the Canterbury earthquake sequence (e.g., densification) did not have a discernible influence on the liquefaction susceptibility of the site in subsequent earthquakes. We suggest that the liquefaction susceptibility of the study sites during pre-CES liquefaction is unlikely to have been modified significantly by sediment densification.

The surface at site 1 has aggraded by ~ 20 cm since excavation of the pits (Figs. 3, 4, and 5),

suggesting that the site was still actively aggrading following the pre-Canterbury earthquake sequence event. The geometry of the pre-Canterbury earthquake sequence dikes at site 1 suggests ~ 70 – 90 cm of sedimentation may be inferred at the site since the paleoearthquake. This inferred sedimentation may have increased the overburden pressure on the liquefiable strata, increasing the cyclic stress threshold required to initiate liquefaction and therefore decreasing the liquefaction susceptibility of the site. The sediment accumulation at site 2 cannot be directly calculated; however, historical records of periodic flooding (Cowie, 1957) suggest that sedimentation has most likely occurred at the site since the paleoearthquake. Any compaction of subsurface strata during the previous episodes of liquefaction is unlikely to have had a major effect on liquefaction susceptibility. The inferred sedimentation, limited compaction, and combined limited cementation, suggest that the liquefaction triggering threshold during the earthquake(s) forming the pre-Canterbury earthquake sequence liquefaction features in Avonside is likely to have been consistent or lower than that during the Canterbury earthquake sequence.

IMPLICATIONS FOR PALEOSEISMIC STUDIES AND FUTURE LAND USE

The identification of pre-Canterbury earthquake sequence liquefaction at both sites in Avonside indicates that residential development within eastern Christchurch (ca. 1860–2005) took place on top of sediments where geologic evidence for liquefaction was present in the shallow subsurface. The identification of the pre-Canterbury earthquake sequence at both sites in Avonside highlights the potential of paleoliquefaction investigations, in addition to geotechnical data, to contribute to land-use planning. Future residential and commercial developments could therefore utilize paleoliquefaction observations to assist with making informed decisions on land zonation and building design criteria.

The approximate alignment of the pre-Canterbury earthquake sequence features with the ~ 25 -cm-wide lateral spreading fissure at site 1 and the ~ 5 -cm-wide dike at site 2 indicates that some zones of weakness were reoccupied during the subsequent earthquake events (Figs. 3, 5, and 10). The identification of two generations of Canterbury earthquake sequence liquefaction within the subsurface at both sites (Figs. 8 and 10), despite the 10 Canterbury earthquake sequence liquefaction events recorded at site 2 (Quigley et al., 2013), suggests that geologic evidence for paleoliquefaction may significantly

underrepresent the number of distinct liquefaction events at the site. Feeder dike generations identified in paleoliquefaction studies should therefore be generally treated as proxies for the minimum number of liquefaction-inducing earthquakes.

The CPTu and hand auger data indicate that the widest Canterbury earthquake sequence dike (>50 cm) identified on the floor of T2 at site 1 (Fig. 4C) likely formed during the February 2011 earthquake and was likely sourced from a greater depth than the other Canterbury earthquake sequence dikes. The width of this dike (>50 cm) compared to the other Canterbury earthquake sequence (<25 cm) and pre-Canterbury earthquake sequence dikes (<7 cm) implies that the shaking intensity and severity of liquefaction experienced during the February 2011 earthquake is likely to have been the most severe since initial deposition of the fluvial sediment ca. A.D. 665. The width of liquefaction dikes preserved within the subsurface may act as proxies for the intensity of shaking and associated severity of liquefaction experienced during historic earthquakes in certain instances.

CONCLUSIONS

Canterbury earthquake sequence liquefaction features at sites 1 and 2 consist of liquefaction dikes and sills that exhibit subvertical, planar morphology and increase in width with depth. The dikes and sills are composed of gray, well-sorted, fine to medium sand that lacks the oxidation and mottling developed in the surrounding sediment. Pre-Canterbury earthquake sequence liquefaction features were also identified at both sites, including dikes at site 1 and an injection feature at site 2. These pre features were distinguished from the Canterbury earthquake sequence features by their oxidized and mottled appearance and bioturbated contacts.

The presence of pre-Canterbury earthquake sequence liquefaction confirms that earthquake-induced strong ground motions exceeding the threshold value for liquefaction occurred within eastern Christchurch prior to the 2010 Darfield earthquake. Crosscutting relationships combined with ^{14}C dating at site 1 indicate that this event most likely occurred between A.D. 1660–1803 (S2) and ca. 1905.

The $\text{PGA}_{7.5}$ values calculated for site 1 for the five historic events indicate that only the 1869 Christchurch earthquake generated ground motions in excess of the local liquefaction triggering threshold of $\text{PGA}_{7.5} \sim 0.06g$ (Quigley et al., 2013). The recorded damage within Avon-side during the event (MMI 7) and reports of the tide running up the Heathcote River support the inference that liquefaction may have been trig-

gered during this event. The calculated $\text{PGA}_{7.5}$ for this event corresponds with minor liquefaction in the Canterbury earthquake sequence. This supports the interpretation that minor liquefaction in highly susceptible sediments may have formed during this event.

The documentation of liquefaction in moderate-to-large ($M_w \sim 5\text{--}7.9$) earthquakes at distances exceeding that predicted by Ambraseys (1988) (i.e., ~ 8 km from epicenter for the October 2011 M_w 5.0 earthquake, ~ 14 km from epicenter for the April 2011 M_w 5.0 earthquake, and ~ 6 km from inferred epicenter for the 1869 Christchurch M_w 4.8 \pm 0.1 earthquake) indicates that even moderate M_w earthquakes on blind faults can trigger liquefaction in highly susceptible sediments or in areas prone to seismic amplification at distances greater than predicted. More data documenting the spatial distribution of liquefaction associated with moderate M_w earthquakes will help to better refine the liquefaction hazard posed by earthquakes of this nature.

ACKNOWLEDGMENTS

We thank Martitia Tuttle, Peter Almond, and Pilar Villamor for their discussions and assistance that aided in the interpretation of these pre-Canterbury earthquake sequence liquefaction features. We also thank Matthew Hughes for his assistance with ArcGIS and Brendon Bradley for calculating the peak ground accelerations for the paleoearthquake events. This work was funded by an EQC Capability Fund and the University of Canterbury Mason Trust Fund.

REFERENCES CITED

- Aitken, M.J., 1998, *Introduction to Optical Dating*: Oxford, UK, Oxford University Press, 267 p.
- Almond, P., Villamor, P., Tuttle, M., Langridge, R., Clark, K., Eger, A., Bastin, S., Quigley, M., Barker, P., and Vandergoes, M., 2013, Liquefaction induced by the 2010–2011 Canterbury earthquake sequence and implications of recently discovered paleoliquefaction features: *Geological Society of America Abstracts with Programs*, v. 44, no. 7, p. 414.
- Ambraseys, N.N., 1988, *Engineering seismology part 1: Earthquake Engineering & Structural Dynamics*, v. 17, no. 1, p. 1–50, doi:10.1002/eqe.4290170101.
- Bastin, S.H., Quigley, M.C., Bassett, K., and Green, R.A., 2013, Characterisation of modern and paleo-liquefaction features in eastern Christchurch, NZ, following the 2010–2011 Canterbury earthquake sequence: *NZ Geomechanics News*, v. 26, p. 38–46.
- Berrill, J.B., Mulqueen, P.C., and Ooi, E.T.C., 1994, Liquefaction at Kaiapoi in the 1901 Cheviot, New Zealand, earthquake: *Bulletin of the New Zealand National Society for Earthquake Engineering*, v. 24, no. 3, p. 178–189.
- Bradley, B., 2013, A New Zealand-specific pseudospectral acceleration ground-motion prediction equation for active shallow crustal earthquakes based on foreign models: *Bulletin of the Seismological Society of America*, v. 103, no. 3, p. 1801–1822, doi:10.1785/0120120021.
- Bremer, J., 1985, *Wool Scours of New Zealand—Tales of the Early Industry*: Christchurch, New Zealand, New Zealand Woolscours Association Inc., 136 p.
- Brown, L.J., and Weeber, J.H., 1992, *Geology of the Christchurch Urban Area*: Institute of Geological and Nuclear Sciences Geological Map 1, scale 1:25,000, 1 sheet + 105 p.
- Counts, R.C., and Obermeier, S.F., 2012, Subtle seismic signatures: Using small-scale features and ground fractures as indicators of paleoseismicity, in Cox, R.T., Tuttle, M.P., Boyd, O., and Locat, J., eds., *Recent Advances in North American Paleoseismology and Neotectonics East of the Rockies*: Geological Society of America Special Paper 493, p. 203–219.
- Cowan, H.A., 1991, The North Canterbury earthquake of September 1, 1888: *Journal of the Royal Society of New Zealand*, v. 21, p. 1–12, doi:10.1080/03036758.1991.10416105.
- Cowie, C.A., 1957, *Floods in New Zealand 1920–1953, with Notes on Some Earlier Floods*: Wellington, New Zealand, The Soil Conservation and Rivers Control Council, 240 p.
- Cox, S.C., Rutter, H.K., Sims, A., Manga, M., Weir, J.J., Ezzy, T., White, P.A., Horton, T.W., and Scott, D., 2012, Hydrological effects of the M_w 7.1 Darfield (Canterbury) earthquake, 4 September 2010: *New Zealand Journal of Geology and Geophysics*, v. 55, no. 3, p. 231–247, doi:10.1080/00288306.2012.680474.
- Cubrinovski, M., and Green, R.A., eds., 2010, *Geotechnical Reconnaissance of the 2010 Darfield (Canterbury) Earthquake* (contributing authors: Allen, J., Ashford, S., Bowman, E., Bradley, B., Cox, B., Cubrinovski, M., Green, R., Hutchinson, T., Kavazanjian, E., Orense, R., Pender, M., Quigley, M., Wotherspoon, L.): *Bulletin of the New Zealand Society for Earthquake Engineering*, v. 43, no. 4, p. 243–320.
- Cubrinovski, M., Bray, J.D., Taylor, M., Giorgini, S., Bradley, B., Wotherspoon, L., and Zupan, J., 2011, Soil liquefaction effects in the Central Business District during the February 2011 Christchurch earthquake: *Seismological Research Letters*, v. 82, no. 6, p. 893–904, doi:10.1785/gssrl.82.6.893.
- Downes, G., and Yetton, M., 2012, Pre-2010 historical seismicity near Christchurch, New Zealand: The 1869 M_w 4.7–4.9 Christchurch and 1870 M_w 5.6–5.8 Lake Ellesmere earthquakes: *New Zealand Journal of Geology and Geophysics*, v. 55, no. 3, p. 199–205, doi:10.1080/00288306.2012.690767.
- Elder, D.M., McCahon, I.F., and Yetton, M.D., 1991, *The Earthquake Hazard in Christchurch: A Detailed Evaluation: Research Report to the EQC: Christchurch, New Zealand, Soils and Foundations Ltd*, 131 p.
- Galli, P., 2000, New empirical relationships between magnitude and distance for liquefaction: *Tectonophysics*, v. 324, p. 169–187, doi:10.1016/S0040-1951(00)00118-9.
- Green, R.A., Obermeier, S.F., and Olsson, S.M., 2005, Engineering geologic and geotechnical analysis of paleoseismic shaking using liquefaction effects: Field examples: *Engineering Geology*, v. 76, p. 263–293, doi:10.1016/j.enggeo.2004.07.026.
- Hjølström, F., 1939, Transportation of detritus by moving water: Part 1. Transportation, in Trask, P.D., ed., *Recent Marine Sediments: American Association of Petroleum Geologists Special Volume 10*, p. 5–31.
- Howard, M.E., Nicol, A., Campbell, J., and Pettinga, J., 2005, Holocene paleoearthquakes on the strike-slip Porters Pass fault, Canterbury, New Zealand: *New Zealand Journal of Geology and Geophysics*, v. 48, no. 1, p. 59–74, doi:10.1080/00288306.2005.9515098.
- Idriss, I.M., and Boulanger, R.W., 2008, *Soil Liquefaction during Earthquakes*, Monograph Series: Oakland, California, Earthquake Engineering Research Institute, 261 p.
- Loope, D.B., Elder, J.F., Zlotnik, V.A., Kettler, R.M., and Pederson, D.T., 2013, Jurassic earthquake sequence recorded by multiple generations of sand blows, Zion National Park, Utah: *Geology*, v. 41, no. 10, p. 1127–1134.
- McCormac, F.G., Hogg, A.G., Blackwell, P.G., Buck, C.E., Higham, T.F.G., and Reimer, P.J., 2004, SHCAL04 Southern Hemisphere calibration, 0–11.0 cal kyr BP: *Radiocarbon*, v. 46, no. 3, p. 1087–1092.
- Montenat, C., Barrier, P., d'Estevou, P.O., and Hibsich, C., 2007, Seismites: An attempt at critical analysis and classification: *Sedimentary Geology*, v. 196, p. 5–30, doi:10.1016/j.sedgeo.2006.08.004.
- NZS 1170.5, 2004, *Structural Design Actions Part 5: Earthquake Actions*: Wellington, New Zealand, Standards New Zealand, 80 p.

- Obermeier, S.F., 1996, Use of liquefaction-induced features for paleoseismic analysis—An overview of how seismic liquefaction features can be distinguished from other features and how their regional distribution and properties of source sediment can be used to infer the location and strength of Holocene paleo-earthquakes: *Engineering Geology*, v. 44, p. 1–76, doi:10.1016/S0013-7952(96)00040-3.
- Obermeier, S.F., Bleuer, N.K., Munson, C.A., Munson, P.J., Martin, W.S., McWilliams, K.M., Tabaczynski, D.A., Odum, J.K., Rubin, M., and Eggart, D.L., 1991, Evidence of strong earthquake shaking in the lower Wabash Valley from prehistoric liquefaction features: *Science*, v. 251, p. 1061–1063, doi:10.1126/science.251.4997.1061.
- Obermeier, S.F., Olson, S.M., and Green, R.A., 2005, Field occurrences of liquefaction-induced features: A primer for engineering geologic analysis of paleoseismic shaking: *Engineering Geology*, v. 76, p. 209–234, doi:10.1016/j.enggeo.2004.07.009.
- Owen, G., and Moretti, M., 2011, Identifying triggers for liquefaction-induced soft-sediment deformation in sands: *Sedimentary Geology*, v. 235, p. 141–147, doi:10.1016/j.sedgeo.2010.10.003.
- Pettinga, J.R., Yetton, M.D., Van Dissen, R.J., and Downes, G., 2001, Earthquake source identification and characteristics for the Canterbury region, South Island, New Zealand: *Bulletin of the New Zealand Society for Earthquake Engineering*, v. 34, no. 4, p. 282–317.
- Quigley, M.C., Bastin, S., and Bradley, B.A., 2013, Recurrent liquefaction in Christchurch, New Zealand, during the Canterbury earthquake sequence: *Geology*, v. 41, n. 5, p. 614.
- Reid, C.M., Thompson, N.K., Irvine, J.R.M., and Laird, T.E., 2012, Sand volcanoes in the Avon-Heathcote estuary produced by the 2010–2011 Christchurch earthquakes: Implications for geological preservation and expression: *New Zealand Journal of Geology and Geophysics*, v. 55, no. 3, p. 249–254, doi:10.1080/00288306.2012.674051.
- Santucci de Magistris, F., Lanzano, G., Forte, G., and Fabrocino, G., 2013, A database for PGA threshold in liquefaction occurrence: *Soil Dynamics and Earthquake Engineering*, v. 54, p. 17–19, doi:10.1016/j.soildyn.2013.07.011.
- Seed, H.B., and Idriss, I.M., 1982, *Ground Motions and Soil Liquefaction during Earthquakes*, Monograph Series: Berkeley, California, Earthquake Engineering Research Institute, 134 p.
- Silby, K., compiler, 1856, *Christchurch Area Showing Waterways Swamps and Vegetation*: Christchurch Drainage Board, available at <http://resources.ccc.govt.nz/files/blackmap-environmentecology.pdf> (accessed June 2013).
- Sims, J.D., 1975, Determining earthquake recurrence intervals from deformational structures in young lacustrine sediments: *Tectonophysics*, v. 29, p. 141–152, doi:10.1016/0040-1951(75)90139-0.
- Sims, J.D., and Garvin, C.D., 1995, Recurrent liquefaction induced by the 1989 Loma Prieta earthquake and 1990 and 1991 aftershocks: Implications for paleoseismicity studies: *Bulletin of the Seismological Society of America*, v. 85, no. 1, p. 51–65.
- Stirling, M., Yetton, M., Pettinga, J., Berryman, K.R., and Downes, G.L., 1999, Probabilistic Seismic Hazard Assessment and Earthquake Scenarios for the Canterbury Region, and Historic Earthquakes in Christchurch. Stage 1 (Part B) of Canterbury Regional Council's Earthquake Hazard and Risk Assessment Study: Lower Hutt, New Zealand, Institute of Geological and Nuclear Sciences Client Report 1999/53, GNS Science, 14 p.
- Stirling, M., Gerstenberger, M., Litchfield, N., McVerry, G., Smith, W., Pettinga, J., and Barnes, P., 2008, Seismic hazard of the Canterbury region, New Zealand: New earthquake source model and methodology: *Bulletin of the New Zealand Society for Earthquake Engineering*, v. 41, no. 2, p. 51–67.
- Stirling, M., McVerry, G., Gerstenberger, M., Litchfield, N., Van Dissen, R., Berryman, K., Barnes, P., Wallace, L., Villamor, P., Langridge, R., Lamarche, G., Nodder, S., Reyners, M., Bradley, B., Rhoades, D., Smith, W., Nicol, A., Pettinga, J., Clark, K., and Jacobs, K., 2012, National seismic hazard model for New Zealand: 2010 update: *Bulletin of the Seismological Society of America*, v. 102, no. 4, p. 1514–1542.
- Sutherland, R., Eberhart-Phillips, D., Harris, R.A., Stern, T.A., Beavan, R.J., Ellis, S.M., Henrys, S.A., Cox, S.C., Norris, R.J., Berryman, K.R., Townend, J., Bannister, S.C., Pettinga, J., Leitner, B., Wallace, L.M., Little, T.A., Cooper, A.F., Yetton, M., and Stirling, M.W., 2007, Do great earthquakes occur on the Alpine fault in central South Island, New Zealand?, in Okaya, D.A., Stern, T.A., and Davey, F.J., eds., *A Continental Plate Boundary: Tectonics at South Island, New Zealand*: American Geophysical Union Geophysical Monograph 175, p. 235–251.
- Tuttle, M., 2001, The use of liquefaction features in paleoseismology: Lessons learnt in the New Madrid seismic zone, central United States: *Journal of Seismology*, v. 5, p. 361–380, doi:10.1023/A:1011423525258.
- Tuttle, M.P., and Atkinson, G.M., 2010, Localization of large earthquakes in the Charlevoix seismic zone, Quebec, Canada, during the past 10,000 years: *Seismological Research Letters*, v. 81, no. 1, p. 140–147, doi:10.1785/gssrl.81.1.140.
- Tuttle, M., and Barstow, N., 1996, Liquefaction-related ground failure: A case study in the New Madrid seismic zone, central United States: *Bulletin of the Seismological Society of America*, v. 86, no. 3, p. 636–645.
- Tuttle, M.P., and Hartleb, R., 2012, CEUS Paleo-liquefaction Database, Uncertainties Associated with Paleoliquefaction Data, and Guidance for Seismic Source Characterization: Central and Eastern United States Seismic Source Characterization for Nuclear Facilities, Appendix E. NUREG-2115, Volume 5: Appendices C to F: Palo Alto, California, U.S. Department of Energy (DOE), U.S. Nuclear Regulatory Commission (NRC), and Electric Power Research Institute (EPRI), Accession No. ML12048A859.
- Tuttle, M.P., Schweig, E.S., Sims, J.D., Lafferty, R.H., Wolf, L.W., and Haynes, M.L., 2002, The earthquake potential of the New Madrid seismic zone: *Bulletin of the Seismological Society of America*, v. 92, no. 6, p. 2080–2089, doi:10.1785/0120010227.
- Tuttle, M.P., Al-Shukri, H., and Mahdi, H., 2006, Very large earthquakes centered southwest of the New Madrid seismic zone 5,000–7,000 years ago: *Seismological Research Letters*, v. 77, no. 6, p. 755–770, doi:10.1785/gssrl.77.6.755.
- Van Breemen, N., and Burman, P., 2002, *Soil Formation* (2nd ed.): Dordrecht, Netherlands, Kluwer Academic Publishers, 408 p.

SCIENCE EDITOR: A. HOPE JAHREN
ASSOCIATE EDITOR: STEPHEN T. JOHNSTON

MANUSCRIPT RECEIVED 26 JULY 2014
REVISED MANUSCRIPT RECEIVED 12 DECEMBER 2014
MANUSCRIPT ACCEPTED 25 FEBRUARY 2015

Printed in the USA